frontiers | Frontiers in Batteries and Electrochemistry

TYPE Review
PUBLISHED 23 August 2024
DOI 10.3389/fbael.2024.1422400

OPEN ACCESS

EDITED BY
Abhishek Lahiri,
Brunel University London, United Kingdom

REVIEWED BY
Bing Ding,
Nanjing University of Aeronautics and Astronautics, China
Gopal Ramalingam,
Alagappa University, India

*CORRESPONDENCE
Lok Kumar Shrestha,
shrestha.lokkumar@nims.go.jp
Katsuhiko Ariga,
ariga.katsuhiko@nims.go.jp

RECEIVED 23 April 2024
ACCEPTED 13 August 2024
PUBLISHED 23 August 2024

CITATION
Shrestha LK and Ariga K (2024) Nanoarchitectonics for supercapacitor: biomass vs. fullerene.
Front. Batteries Electrochem. 3:1422400.
doi: 10.3389/fbael.2024.1422400

Nanoarchitectonics for supercapacitor: biomass vs. fullerene

Lok Kumar Shrestha[1,2]* and Katsuhiko Ariga[1,3]*

[1]Research Center for Materials Nanoarchitectonics (MANA), National Institute for Materials Science (NIMS), Tsukuba, Japan, [2]Department of Materials Science, Institute of Pure and Applied Sciences, University of Tsukuba, Tsukuba, Japan, [3]Department of Advanced Materials Science, Graduate School of Frontier Sciences, The University of Tokyo, Chiba, Japan

The recognition of the importance of nanostructures is mainly due to the development of nanotechnology. For further developments in materials sciences, a concept that integrates nanotechnology with material chemistry to fabricate functional materials has to be proposed. Nanoarchitectonics will carry out this task. In nanoarchitectonics, we architect functional material systems from nano-units (atoms, molecules, nanomaterials). The methodology is not specific to any particular material or application. It covers a wide range. Therefore, nanoarchitectonics can be thought of as the method for everything in materials science. As typical demonstrations for usages of nanoarchitectonics, this review paper presents our work on nanoarchitectonics for supercapacitors. We divide it into two categories with different approaches. The first is the development of carbon materials as supercapacitor electrode materials from biomass. The second category is preparing carbon materials using structures created by supramolecular assembly of fullerenes such as C_{60} and C_{70}. By presenting examples using opposite starting materials, a complex natural material, and an ultimately simple molecule, we will demonstrate the versatility and breadth of possibilities of this approach.

KEYWORDS

biomass, carbon, crystal, fullerene, liquid-liquid interface, nanoarchitectonics, supercapacitor, supramolecular assembly

1 Introduction

Many problems exist in today's society, such as energy, environment, and medicine. Solving these problems requires the development of materials and systems assembled from them that can meet those demands. Especially, there is a tremendous interest in energy issues that support expanded human activities. In addition to solar cells (Kojima et al., 2009; Kinoshita, 2022), fuel cells (Islam et al., 2022; Huang H. et al., 2024), and various ion batteries (Yoshino, 2022; Hosaka and Komaba, 2022), there are high expectations for supercapacitors (Zhang et al., 2023; Shinde et al., 2023a). What underlies these energy devices is the development of materials that enhance their functions. One of the essential keys to solving energy problems lies in material chemistry.

More fundamentally, human development has been accompanied by the progress of materials science. People have obtained materials from the natural world and processed them to create useful tools. In the 20th century, various disciplines related to materials production were established. These are organic chemistry, inorganic chemistry, coordination chemistry, polymer chemistry, supramolecular chemistry, biochemistry,

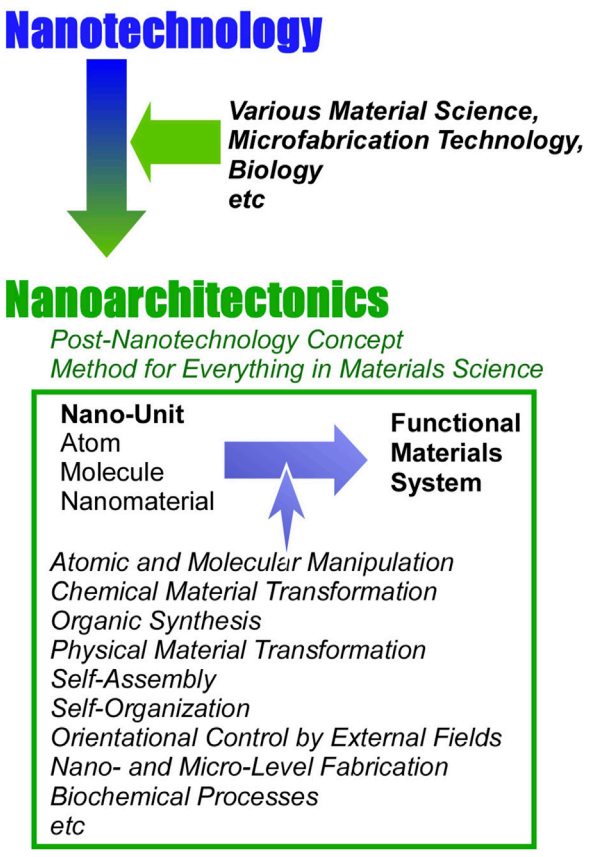

FIGURE 1
Outline of nanoarchitectonics concept.

and other material chemistry, which gave mankind knowledge and ways to design and rationally synthesize desired substances. The creation of the discipline has greatly increased the speed at which functional substances can be developed. As functional material systems were developed, one fact became apparent. It is not only the materials themselves but also the material's structure that is extremely important in expressing its function. In particular, control of the nano-level structure is important. Such knowledge is paramount in current research on energy materials development (Guo et al., 2016; Imahori, 2023).

The recognition of the importance of nanostructures is mainly due to the development of nanotechnology. Nanotechnology techniques have made it possible to directly observe and manipulate atoms, molecules, and nano-objects (Sugimoto et al., 2007; Sun et al., 2023). It is also possible to measure physical properties at the nanoscale (Kimura et al., 2019; Tokura and Kanazawa, 2021). It has been found that there are unique physical properties, such as quantum effects at the nanoscale (Shimohata et al., 2023; Saitow, 2024). In addition, when functional components are rationally organized, their functions change dramatically. Signals, energy, electrons, and chemical signals can flow asymmetrically or be harvested. Functions beyond those of devices developed by microfabrication techniques are demonstrated in nanomaterial systems and devices that are controlled by nanoscale phenomena (Ishii et al., 2023; Kalyana Sundaram et al., 2023). This point in energy-related materials and devices is also important.

The importance of nanostructures in developing functional materials is widely recognized, and that has to be supported by establishing a new concept. In other words, a concept that integrates nanotechnology with material chemistry to fabricate functional materials has to be proposed. This task will be carried out by nanoarchitectonics (Figure 1) (Ariga et al., 2015; Aono and Ariga, 2016), which has recently gained much attention. As Richard Feynman initiated nanotechnology in the middle of the 20th century (Feynman, 1960; Roukes, 2007), nanoarchitectonics was proposed by Masakazu Aono at the beginning of the 21st century (Chaikittisilp et al., 2022; Ariga, 2023a). Therefore, nanoarchitectonics can be considered a post-nanotechnology concept (Ariga, 2021). Methods such as nanoarchitectonics were also considered in fields such as supramolecular chemistry and materials science (Ariga et al., 2019; Liu S. et al., 2023). Therefore, rather than pioneering something completely new, nanoarchitectonics is more of an integration of existing scientific fields. Nanoarchitectonics is an attempt to integrate nanotechnology with various fields of material science, microfabrication technology, and biology. Nanoarchitectonics is the process of building functional materials based on knowledge at the nano-level (Ariga, 2023b).

In nanoarchitectonics, we architect functional material systems from nano-units (atoms, molecules, nanomaterials). In doing so, it successfully selects or combines various methods from various research fields (Ariga et al., 2016). The elemental processes include atomic and molecular manipulation, chemical material transformation, organic synthesis, physical material transformation, self-assembly, self-organization, orientational control by external fields, nano- and micro-level fabrication, and biochemical processes. For example, thin-film fabrication techniques such as Langmuir-Blodgett (LB) method (Oliveira et al., 2022; Ariga, 2023c) and layer-by-layer (LbL) assembly (Ariga et al., 2022; Ariga et al., 2024) are used in combination to architect functional material systems. Rather than creating materials through self-assembly by simple equilibrium, nanoarchitectonics combines several processes and is better suited for building asymmetric and hierarchical functional structures (Ariga et al., 2020). In other words, it is a methodology suitable for building more functional complex systems.

The above nanoarchitectonics methodology is not specific to any particular material or application. It covers a wide range. Nanoarchitectonics is a methodology for building functional materials from nano units, such as atoms and molecules. Originally, all matter is made of atoms and molecules. Therefore, nanoarchitectonics is a concept that can be applied to manufacture all matter. In analogy to the theory of everything (Laughlin and Pines, 2000), which is the ultimate theory of physics, nanoarchitectonics can be thought of as the method for everything in materials science (Ariga and Fakhrullin, 2022; Ariga, 2024). In fact, there are a variety of recent papers advocating nanoarchitectonics. It is also used in fundamental fields such as material synthesis (Hikichi et al., 2023; Huang P. et al., 2024), structure fabrication (Cao et al., 2022; Eftekhari et al., 2024), basic physics (Nayak et al., 2018; Eguchi et al., 2021), and biochemistry (Kalinova et al., 2022; Shen et al., 2022). On the other hand, there are also reports of its use in catalysis (Chen et al., 2021a;

Sharma et al., 2024), sensors (Chen et al., 2022a; Kim et al., 2023), devices (Tsuchiya et al., 2022; Azzaroni et al., 2023), environmental remediation (Prasanthi et al., 2022; Tipplook et al., 2024), drug delivery (Reddy et al., 2023; Zhang et al., 2024), cell control (Hu et al., 2022; Jia et al., 2023), and medical applications (Sutrisno and Ariga, 2023; Meng et al., 2024). The use of nanoarchitectonics in the energy field, where material development is a very powerful factor, is remarkable. It is used in solar cells (Liu X. et al., 2021; Bogachuk et al., 2023), fuel cells (Thmaini et al., 2023; Liang et al., 2024), batteries (Chen et al., 2016; Koralkar et al., 2024), and their elemental technologies (Kim et al., 2017; Chen et al., 2022b), as well as in supercapacitor applications (Shinde et al., 2023b; Wang et al., 2024).

Against this background, this review paper presents our work on nanoarchitectonics for supercapacitors. We divide it into two categories with different approaches. The first is the development of carbon materials as supercapacitor electrode materials from biomass (Shrestha et al., 2023a; Zhang and Peng, 2024). This category presents the preparation of carbon materials from natural materials with complex components, such as plant seeds, as starting materials, and the development of enhanced energy storage supercapacitors. The second category is the preparation of carbon materials using structures created by supramolecular assembly of fullerenes such as C_{60} and C_{70} (Shrestha RG. et al., 2020; Munawar et al., 2023). Fullerenes are very simple objects, 0D molecules composed of a single element, carbon. By presenting examples using opposite starting materials, a complex natural material, and an ultimately simple molecule, we will demonstrate the versatility and breadth of possibilities of this approach. The characteristics of these approaches will also be compared in the final section.

2 From biomass

Biomass carbon is a carbon material processed from plant-derived surplus biomass as raw material. Carbon materials derived from the biowaste by activation or carbonization contributes to realizing a recycling-oriented economic society by recycling raw materials (Sagawa et al., 2022; Hassan et al., 2024). Furthermore, it is expected to reduce air pollutants such as PM2.5 and greenhouse gases such as CO_2 emitted from the incineration and disposal of surplus biomass. CO_2 is absorbed by photosynthesis during the process of biomass material generation. This maintains an equilibrium between the CO_2 emitted and the CO_2 used in photosynthesis, and the use of biomass carbon is said to contribute to carbon neutrality (Chapman et al., 2022; Fukushima et al., 2023). It could also lead to a reduction in global environmental impact and prevention of global warming. There has been growing concern to manage the natural biowaste for the sustainable development and to produce energy storage materials. It has been essential to recycle the biowaste into the renewable energy-related applications. Biomass of natural origin can be transformed into the functional carbon materials through various carbonization processes, including physical activation, chemical activation, direct carbonization, etc. Because of the low cost of the precursors (biowaste), the scalability of biomass-derived carbon materials is better than that of carbon prepared from other carbon sources. The scalable materials production is relatively economical compared to the synthetic carbon sources such as fullerene crystals. Surface textural properties of the biomass carbons are tunable depending on the preparation method, activating agents, mixing ratio of the activator and precursor, and the carbonization temperature. The specific surface area can be tuned from a few hundred to a few thousand m^2/g. The yield of the carbon materials depends on the carbonization temperature. Generally, chemical activation with the low energy method, i.e., at low carbonization temperatures (400°C–700°C), leads to the high yield of the carbons, enabling the scalable synthesis of biomass carbon. It can be converted to high energy storage and energy-related applications if its structure and surface textural properties can be skillfully controlled. Biomass-derived ultrahigh surface area carbon materials are being considered as the high-performance electrode materials in supercapacitors. Below are some recent examples of biomass carbons explored as electrode materials for supercapacitors.

Nanoporous activated carbon materials derived from agricultural waste are useful as electrode materials for high-rate performance electrochemical supercapacitors. Shrestha and co-workers have created a high surface area nanoporous activated carbon material from Lapsi (*Choerospondias axillaris*) seeds as an agricultural waste biomass (Shrestha LK. et al., 2020). In addition to the fixed carbon content, moisture content, and volatile matter, the biomass precursors also have ash content. The ash content measures the amount of noncombustible materials contained in the sample, i.e., the minerals left over after removing the moisture and volatile organic materials after high-temperature heat treatments. In other words, it is an industrial by-product obtained as a solid waste generated during the chemical conversion of biomass for energy production. It can be further transformed into a helpful resource. The ash content depends on the biomass itself. From the proximate analysis of Lapsi seed stone powder, the ash content was estimated to be ca. 2.7%. After the chemical activation, the surface morphology studied by scanning electron microscopy (SEM) revealed that the Lapsi-derived carbon exhibits granules of irregular size distributions. The carbon particles ranged from 50 to 300 μm, containing macropores and honeycomb-like surface morphology. Such an irregular shape of the carbon particles is commonly observed in biomass-derived carbon. On the other hand, self-assembled fullerene crystals' well-defined shape and size give porous carbon materials retaining of the shape and size of the starting materials. The high surface area nanoporous carbon material was obtained by activating the raw material with zinc chloride at 700°C. The specific surface areas and pore volumes of the carbon materials are found, in the ranges from 931 to 2,272 $m^2\ g^{-1}$ and 0.998–2.845 $cm^3\ g^{-1}$, respectively. The amorphous structure of the resulting carbonaceous material was confirmed by powder X-ray diffraction and Raman scattering spectroscopy. The presence of oxygen-containing functional groups was also confirmed by Fourier transform infrared spectroscopy, and electron microscopic analysis, including SEM and TEM, revealed the granular nanoporous structure of the material. High-resolution TEM observations revealed a graphitic carbon structure with interconnected mesopores. The surface area and pore volume of this carbon material were found to be superior to the commercially available activated carbons. The working electrode was prepared using these carbon materials, and the electrochemical

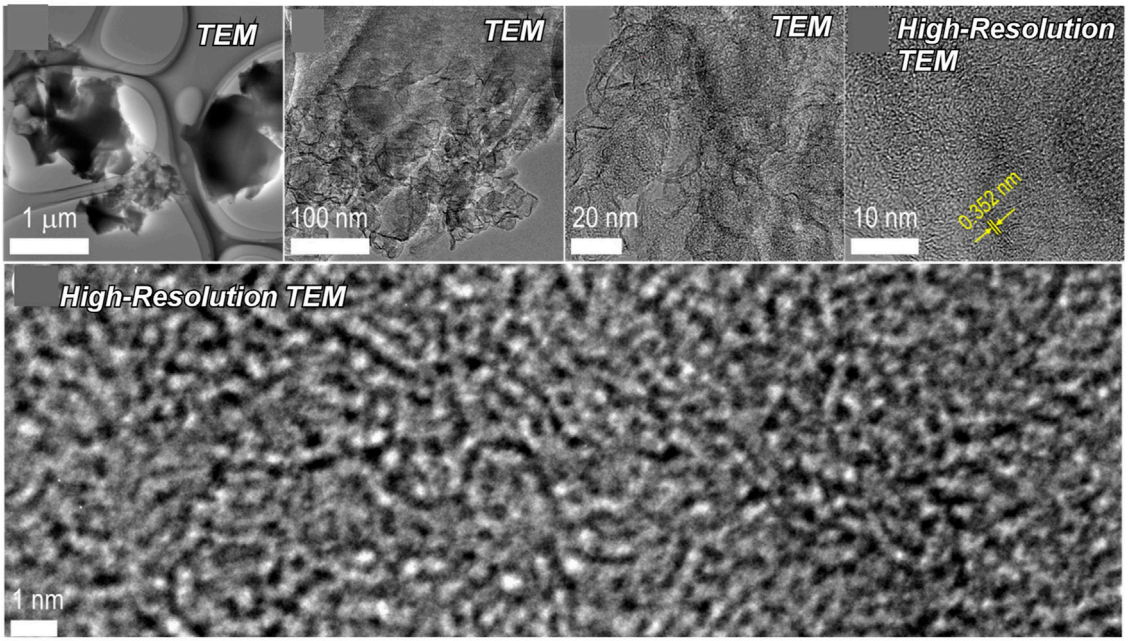

FIGURE 2
SEM, TEM, and high-resolution TEM images of nanoporous carbon prepared from *Phyllanthus emblica* seed by chemical activation with potassium hydroxide at high temperatures under a nitrogen gas atmosphere. Reproduced under terms of the CC-BY license from Shrestha LK. et al. (2022) MDPI.

supercapacitance performance was investigated in a three-electrode cell setup in 1 M H_2SO_4 aqueous electrolyte solution. The electrode prepared with the optimal surface textural properties showed excellent electrochemical supercapacitance performance achieving a high specific capacitance (C_s) of 284 F g^{-1} at a current density of 1 A g^{-1}, followed by a 99% capacity retention after 10,000 charge-discharge cycles. It shows that Lapsi seed can be a potential carbon source for designing high-performance supercapacitor devices.

Nanoporous carbon was prepared from *Phyllanthus emblica* (Amala) seed by chemical activation with a potassium hydroxide (KOH) activator (Shrestha LK. et al., 2022). KOH activation was performed at different temperatures (700°C–1,000°C) under a nitrogen gas atmosphere. The prepared samples are referred to as AmC_K700, AmC_K800, AmC_K900, and AmC_K1000 depending on the carbonization temperature. A reference sample prepared without activation is referred to as AmP_900. The prepared nanoporous carbon has a hierarchical pore structure with micro- and mesopores (Figure 2). Well-developed micro/mesoporous structures were observed in SEM (Shrestha LK. et al., 2022) and TEM images (Figure 2). Low-resolution TEM images showed carbon particles of a few microns in size with a porous structure. On the other hand, the magnified TEM images showed abundant mesopores with graphite backbone. Carbon materials with micro/mesopore structures improve the rate performance of supercapacitor electrodes. Figure 3A shows cyclic voltammograms (CV) of Amala-derived carbons recorded at 50 mV s^{-1}. Quasi-rectangular CV profiles with a rapid current response upon exchange of the potential sweep reveal the carbon electrodes exhibit an electrical double-layer capacitor (EDLC) type energy storage mechanism. The shape of the CV curve of the carbon obtained by the lower temperature carbonization (AmC_K700) deviates from the ideal EDLC behavior. The curve exhibits weak redox peaks at 0.2–0.4 V. This is due to a partial contribution of pseudocapacitance to the EDLC due to oxygen functionalities in the carbon material. The total integral current collection in the CV curve for the 900°C carbonized sample is the highest, inferring the highest energy storage capacity among the studied samples, which can be attributed to the surface area properties. Figure 3B shows the CV profiles of the sample with optimal surface textural properties (AmC_K900) at different scan rates from 5–500 mV s^{-1}. Obviously, the total current output escalates with the sweep rate, sustaining the shape of the CV curves even at 500 mV s^{-1}, demonstrating a fast electrolyte ion transfer to the electrode surface via mesoporous structures followed by excellent reversibility. Figure 3C compares the galvanostatic charge/discharge (GCD) curves measured at a fixed current density of 1 A g^{-1}. Triangular symmetrical GCD profiles with the linear discharge tail complement the EDLC energy storage with a well-balanced energy storage mechanism. The discharge time relates to the energy storage capacity of the electrode. The longest discharge time recorded for the AmC_K900 electrode suggests this sample's highest energy storage capacity, which is in line with CV data. Fast electrolyte ion transfer to the electrode surface is evident with the triangular shape GCD curve retention recorded at a high current density of 50 A g^{-1} (Figure 3D). The directly carbonized sample showed very low specific capacitance (C_s) (9 F g^{-1}). However, due to the KOH activation, the AmC_K900 electrode with optimal surface textural properties achieved a high specific capacitance of 272 F g^{-1} (~30-fold enhancement in the capacitance compared to the reference sample). Figure 3E compares the C_s of all the electrodes vs. current density. The C_s of AmC_K900 is superior at all current

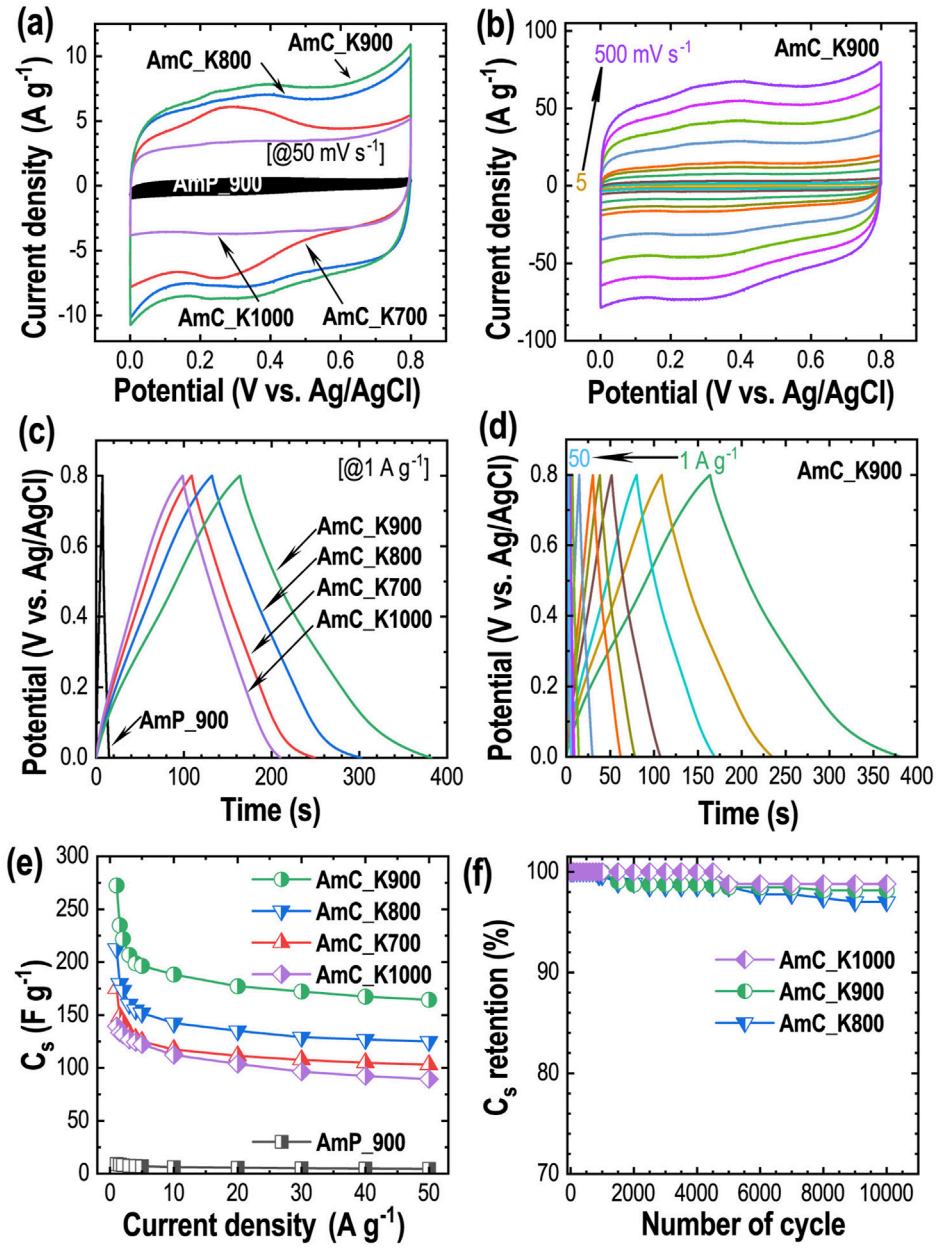

FIGURE 3
Electrochemical supercapacitance performance of nanoporous carbon prepared from *Phyllanthus emblica* seed by chemical activation with potassium hydroxide at high temperatures under a nitrogen gas atmosphere. **(A)** comparison of the CV profiles of reference sample and activated samples recorded at a fixed scan rate of 50 mV s^{-1}, **(B)** CV profiles vs. scan rate for the electrode with the optimal surface textural properties as a typical example, **(C)** comparison of the GCD curves at a fixed current density of 1 A g^{-1}, **(D)** GCD profiles vs. current density for the optimal sample, **(E)** specific capacitance of all samples at different current density, and **(F)** cycle life of the selected electrodes up to 10,000 consecutive charging/discharging cycles. Reproduced under terms of the CC-BY license from Shrestha LK. et al. (2022) MDPI.

densities from 1 to 50 A g^{-1}, followed by AmC_K800 and AmC_K700. The cycle performance of supercapacitors is very crucial in practical energy storage applications. The Amala-derived carbon electrodes showed an excellent cycle life of more than 97% after successive charging/discharging for 10,000 cycles (Figure 3F). Cost-effective manufacturing, rich textural properties, and excellent electrochemical results suggest that *P. emblica* seed is a useful carbon source for the formation of high energy storage supercapacitors.

The inclusion of additional nitrogen functional groups in biomass-derived activated carbon materials with a hierarchical nanoporous structure is expected to further impart superior electrochemical performance. From this perspective, carbon materials based on the *Nelumbo nucifera* (Lotus) seed were developed (Shrestha LK. et al., 2021). A self-nitrogen-doped nanoporous carbon material was prepared from *N. nucifera* seed powder by KOH activation at different temperatures (600°C–1,000°C). This carbon material is an amorphous material

TABLE 1 Surface area, pore volume, and pore sizes of the Lotus seed-derived activated carbon materials obtained by the KOH activation at different temperatures from 600°C to 1,000°C[a]. Reproduced under terms of the CC-BY license from Shrestha LK. et al. (2021) MDPI.

Sample	*SSA* ($m^2\ g^{-1}$)	S_{micro} ($m^2\ g^{-1}$)	S_{meso} ($m^2\ g^{-1}$)	V_p ($cm^3\ g^{-1}$)	V_{micro} ($cm^3\ g^{-1}$)	W_p (nm)	D_p (nm)
LTS_800	46.1	18.8	27.3	0.102	0.044	---	3.09
LTSC_K600	1,059.6	824.5	235.1	0.819	0.472	0.285	3.92
LTSC_K700	1878.4	1,556.1	322.3	1.232	0.775	0.286	3.93
LTSC_K800	2,236.6	1891.3	345.3	1.499	1.034	0.274	3.91
LTSC_K900	2,330.1	1905.7	424.4	1.793	1.206	0.286	3.92
LTSC_K1000	2,489.3	1725.6	763.7	2.384	1.488	0.705	3.93

[a]*SSA*, specific surface area; S_{micro}, surface area contributed from micropores; S_{meso}, surface area of mesopores; V_p, total pore volume; V_{micro}, micropore volume; W_p, micropore size (average half pore width); D_p, mesopore size (average pore diameter).

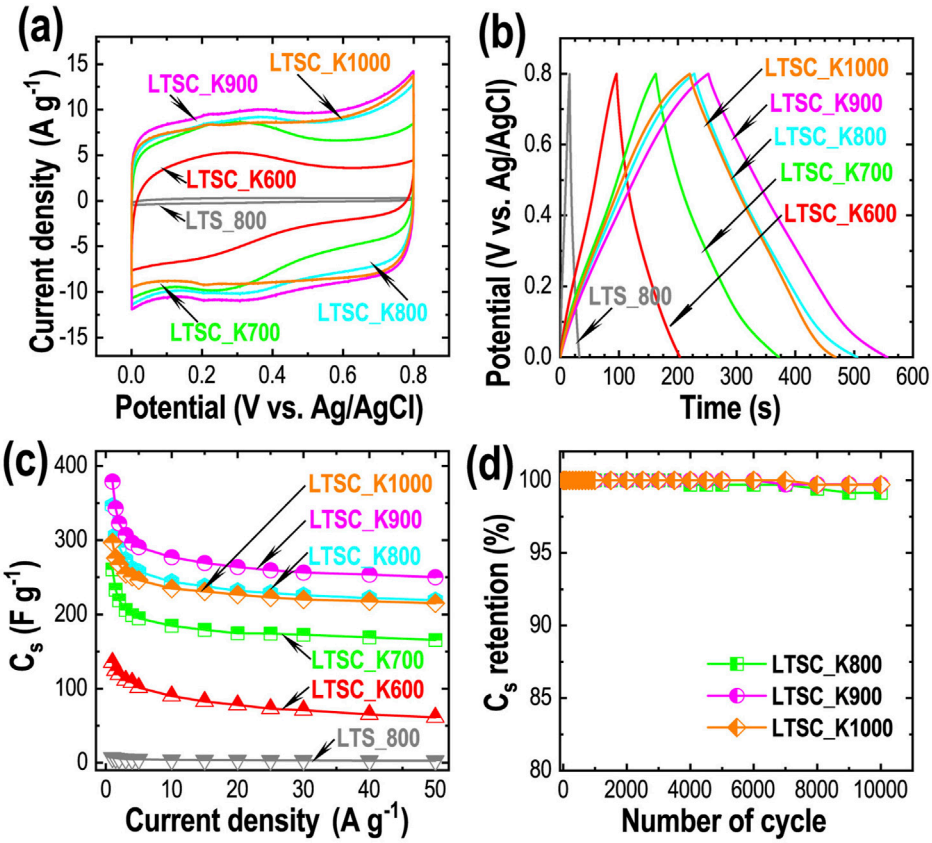

FIGURE 4
Supercapacitance performance of nanoporous carbon prepared from *Nelumbo nucifera* (Lotus) seed by the KOH activation. **(A)** CV profiles of the electrodes prepared with a reference and activated samples recorded 50 mV s^{-1}, **(B)** comparison of the GCD curves at 1 A g^{-1}, which shows that sample activated at 900°C show the longest discharge time inferring highest energy storage capacity, **(C)** specific capacitance of all samples at different current density, and **(D)** cycle life up to 10,000 cycles. Reproduced under terms of the CC-BY license from Shrestha LK. et al. (2021) MDPI.

with a partially graphitic structure containing up to 3.28 atomic% nitrogen. In addition, it has a hierarchical micro- and mesoporous structure. Increasing temperature monotonously increases the total specific surface area. However, there is a maximum in the microporosity. It reaches a maximum at 900°C and then decreases due to the micropore coalescence (Table 1). Thus, the LTSC_K900 offers a much higher electrochemically accessible surface area, promoting ion diffusion through mesopores and electrolyte ion adsorption in the micropores. Inspired by the ultrahigh surface area and self-nitrogen-doping, the electrochemical supercapacitance performances of the Lotus seed-derived activated carbon materials were studied in a three-electrode cell setup. Supercapacitor electrodes made of carbon fabricated under optimized conditions (LTSC_K900) showed excellent electric double-layer capacitor performance. As shown in Figure 4A the total integral current of the LTSC_K900 electrode

is the highest among the studied sample. Similarly, the discharge time of this electrode is the longest, inferring the highest energy storage capacity (Figure 4B). The calculated C_s of the electrode materials shows that due to the lack of porosity, the directly carbonized sample has a very low specific capacitance compared to the KOH-activated samples (Figure 4C). The reference sample without activation showed C_s of only 7.1 F g^{-1} at 1 A g^{-1}, whereas the LTSC_K900 sample achieved the highest specific capacitance of 379.2 F g^{-1}, which can be attributed to the ultrahigh surface area, hierarchically micro-and mesopore architectures and self-nitrogen doping. Furthermore, an extraordinarily long cycle life was achieved with only 0.3% capacity loss after 10,000 charge-discharge cycles (Figure 4D). Electrochemical results indicate that hierarchical porous carbon with nitrogen functionality from *N. nucifera* seed has significant potential as an electric double-layer capacitor electrode material for high-performance supercapacitor applications. Hierarchical porous carbon from *N. nucifera* seed could be a novel and low-cost precursor for large-scale production of carbon materials with self-nitrogen doping. The resulting carbon materials have great potential as electrode materials for high-performance energy storage supercapacitors.

Hierarchical nanoporous activated carbon with a large surface area was prepared by KOH activation and high-temperature carbonization of *Phoenix dactylifera* seed as an agricultural waste (Shrestha RG. et al., 2022). The nanoporous activated carbon obtained from this biomass has a very large surface area and a large pore volume. This excellent surface porosity is due to its interconnected micro- and mesoporous structure. Due to this excellent surface property, this biomass carbon hierarchical nanoporous material has excellent electrochemical charge storage capacity as a supercapacitor electrode material. This hierarchical nanoporous activated carbon has ample potential as an electrode material for commercial and advanced supercapacitors. It is particularly important to consider the activation process and choice of activator to produce a material with a large surface area and optimal pore size distribution. This example demonstrates the importance of KOH activation in the preparation of large surface area activated carbon from biomass for the development of advanced energy storage devices.

Nanoporous activated carbon was synthesized by activation of *Terminalia bellirica* (Barro) seed stone, a biowaste, with zinc chloride ($ZnCl_2$) (Gnawali et al., 2023a). Activation was carried out at relatively low temperatures (400°C–700°C) under an inert nitrogen gas atmosphere. The synthesized carbon material showed well-developed porosity. In particular, the material with the optimal surface area exhibited excellent iodine and methylene blue adsorption properties. Energy storage supercapacitance performance was also investigated, and high specific capacitance was obtained. In short, electrochemical measurements revealed excellent energy storage supercapacitance performance. *Terminalia bellirica* seed is also an important carbon source for producing porous carbon materials with high surface area, which is desired for adsorption technology and high-performance supercapacitor applications.

Ultra-high surface area nanoporous carbon materials with hierarchical micro- and mesopore structures were prepared from *Artocarpus heterophyllus* seeds (Maji et al., 2021a). In this method, the KOH activation method was performed at high temperatures, 600°C–1,000°C. Low-magnification SEM images of all materials prepared show similar microstructures with micron-sized pores on the surface of irregular granular particles (Figure 5). The surface morphology was quite different from that of the KOH-activated samples compared to those carbonized as is. In other words, KOH activation produced an ultra-high surface area nanoporous carbon material with a hierarchical porous structure in which micropores and mesopores coexist. The ultra-high surface area, large pore volume, and hierarchical micro- and mesopore structure of the material enabled it to function as a high-rate performance electrode material for supercapacitors. The experimental results suggest fast electrolyte ion diffusion of near the electrode surface. These behaviors were verified using molecular simulations. The simulation results showed that the capacitance increases as the electrolyte enters the pores. On the other hand, the charging rate was found to be lower than that of the nonporous electrode. However, the mobility of ions in the mesoporous and electric double-layer regions was similar to that of the bulk. Carbon materials with high surface area and large porosity with a hierarchical porous structure are preferred as electrode materials for high energy density supercapacitors. Hierarchical porous carbon from Artocarpus heterophyllus seed was experimentally and theoretically proved to have considerable potential to satisfy this requirement.

3 Based on fullerene assembly

Various biomass types of precursors can be tested extensively to obtain a more ideal carbon material. On the other hand, there are other approaches to develop desired carbon materials by nanoarchitectonics from well-understood molecular structures. In particular, morphology-controlled porous carbons containing many mesopores with extended π-electron conjugation are ideal for supercapacitor applications. For example, fullerenes (C_{60}, C_{70}, etc.) are ideal 0D carbon molecules with extended conjugation of π electrons. In contrast to other material-type nanocarbons, such as one-dimensional carbon nanotubes and two-dimensional graphene, fullerenes can easily form a variety of self-assembled structures under controlled conditions. Recently, self-assembled fullerene nanostructures have been investigated as a π-electron carbon source for the design and synthesis of high surface area porous carbon materials (Shrestha et al., 2013a; Bhadra et al., 2022). Fullerenes form various morphologies of self-assembled structures at the liquid-liquid interface and on solid substrates. For example, the corresponding processes can create 0D spheres and particles (Jiang B. et al., 2022; Chen et al., 2022c), 1D nanowhiskers and nanotubes (Miyazawa, 2009; Shrestha et al., 2013b), 2D nanosheets and nanodiscs (Chen et al., 2021b; Song et al., 2022), and 3D nanocubes (Bairi et al., 2017; Xu et al., 2021) and horns (Tang et al., 2019). The fabrications of hierarchical superstructures, such as a combination of these structures, were also reported (Bairi et al., 2016a; Hsieh et al., 2020). Furthermore, these self-assembled fullerene nanostructures can be directly converted into high surface area nanoporous carbon materials by high-temperature heat treatment while retaining their initial morphology. The framework structure, such as graphitic or amorphous, and porosity can be controlled by carefully varying

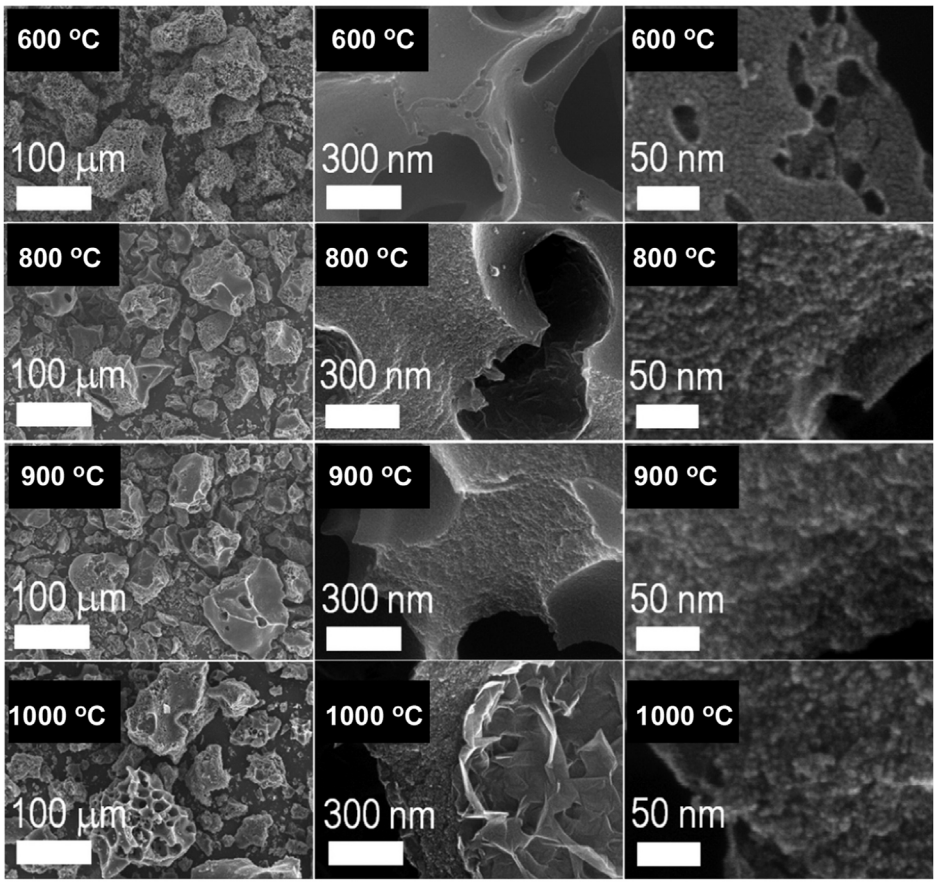

FIGURE 5
SEM images of ultra-high surface area nanoporous carbon materials with hierarchical micro- and mesopore structures prepared from *Artocarpus heterophyllus* seeds at high temperatures, 600, 800, 900, and 1,000°C. Reprinted with permission from Maji et al. (2021a) American Chemical Society.

temperature conditions. The resulting nanoporous carbon materials have a large surface area and excellent electrochemical conductivity. Therefore, they are suitable for applications such as electrode materials for electric double-layer capacitors. Below are some examples of the preparation of carbon materials derived from fullerene assemblies and their supercapacitor applications.

Shrestha and co-workers synthesized self-assembled structures of fullerene C_{60} modulated by the nonionic surfactants of diglycerol monolaurate and diglycerol monomyristate (Shrestha et al., 2016). C_{60} self-assemblies prepared at the liquid-liquid interface consisting of isopropyl alcohol and a saturated solution of C_{60} in ethylbenzene were in the 1D form with well-defined facet structures. On the other hand, when C_{60} crystals were grown in the presence of 1% diglycerol monolaurate or diglycerol monomyristate surfactant in ethyl benzene, the C_{60} self-assembled morphology changed to a kompeito-like morphology with an average diameter of approximately 1.2 μm (Figure 6). This is thought to be an effect of reverse micelles in ethylbenzene. Self-assembled 1D faceted C_{60} crystals and kompeito-like C_{60} crystals showed strong photoluminescence. The photoluminescence maxima were blue-shifted by about 15 nm compared to the original C_{60}. These self-assembled structures could be used to control the optoelectronic properties of fullerene nanostructures. The kompeito-like C_{60} crystals can be converted to highly graphitized nanoporous carbon by high-temperature treatment while maintaining their original morphology. In other words, the kompeito-like crystals were transformed into high surface area nanoporous carbon with a graphitic structure when heat-treated at 2000°C. The heat-treated nanoporous carbon with graphitized strong pore walls has a high surface area. This enhanced the electrochemical supercapacitance performance. The specific capacitance of the carbon sample was about 17 times higher than that of the original kompeito-like C_{60} crystal. In addition, the cycling stability was excellent.

Macaroni-like fullerene crystals were prepared by dynamic liquid-liquid interfacial deposition at room temperature. High-temperature treatment directly converted this structure into mesoporous carbon tubes (Figure 7) (Maji et al., 2021b). During the dynamic liquid-liquid interfacial precipitation process, the C_{60} molecules are not sufficiently present, resulting in a cavity in the center. A hexagonal tube with a solid core in the center is then formed. STEM and TEM analysis confirmed the presence of a solid core in the center and cavities at both ends. Macaroni-like fullerene crystals were heated under a constant flow of nitrogen gas at a high temperature of 900°C to obtain macaroni carbon tubes. The resulting carbon material maintains its initial macaroni-like morphology. High-magnification TEM images confirmed that it

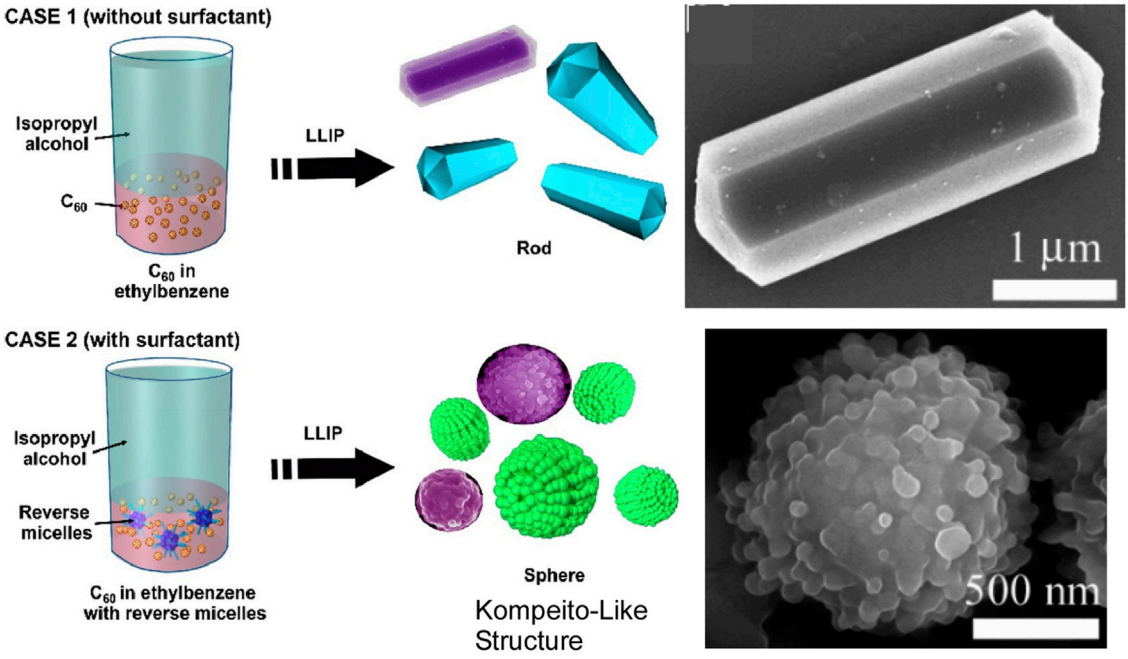

FIGURE 6
(Case 1) C_{60} self-assemblies in the 1D form with well-defined facet structure prepared at the liquid-liquid interface consisting of isopropyl alcohol and a saturated solution of C_{60} in ethylbenzene: (Case 2) C_{60} self-assembled morphology in a kompeito-like morphology with an average diameter of approximately 1.2 µm grown in the presence of 1% diglycerol monolaurate or diglycerol monomyristate surfactant in ethyl benzene. Reprinted with permission from Shrestha et al. (2016) American Chemical Society.

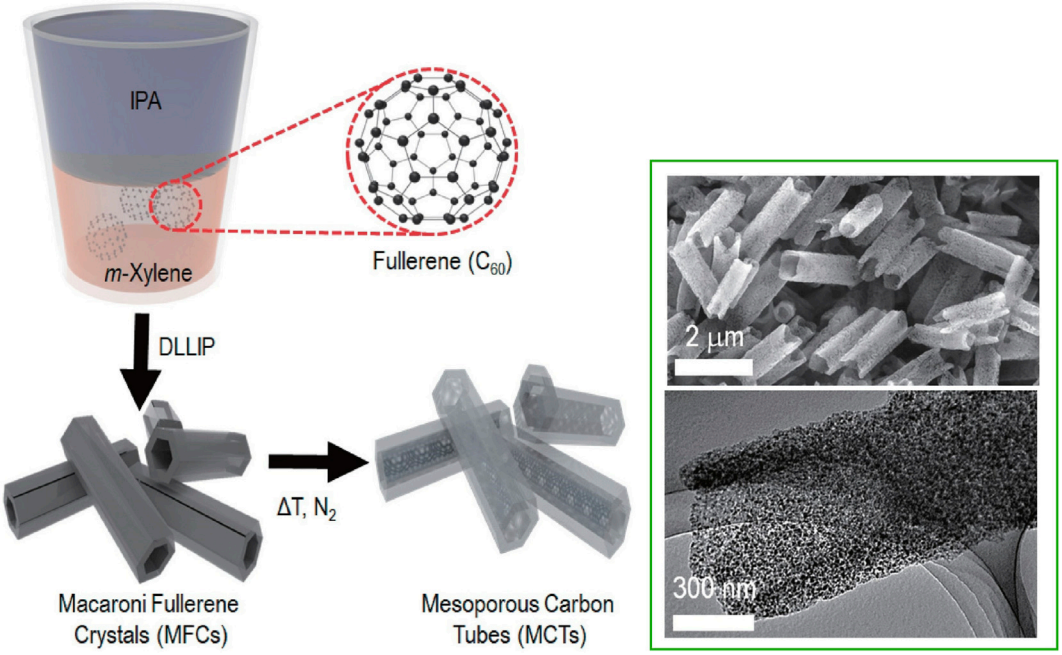

FIGURE 7
Macaroni-like fullerene crystals prepared by the dynamic liquid-liquid interfacial deposition at room temperature, which was directly converted into mesoporous carbon tubes by high-temperature treatment. Reprinted with permission from Maji et al. (2021b) Oxford University Press.

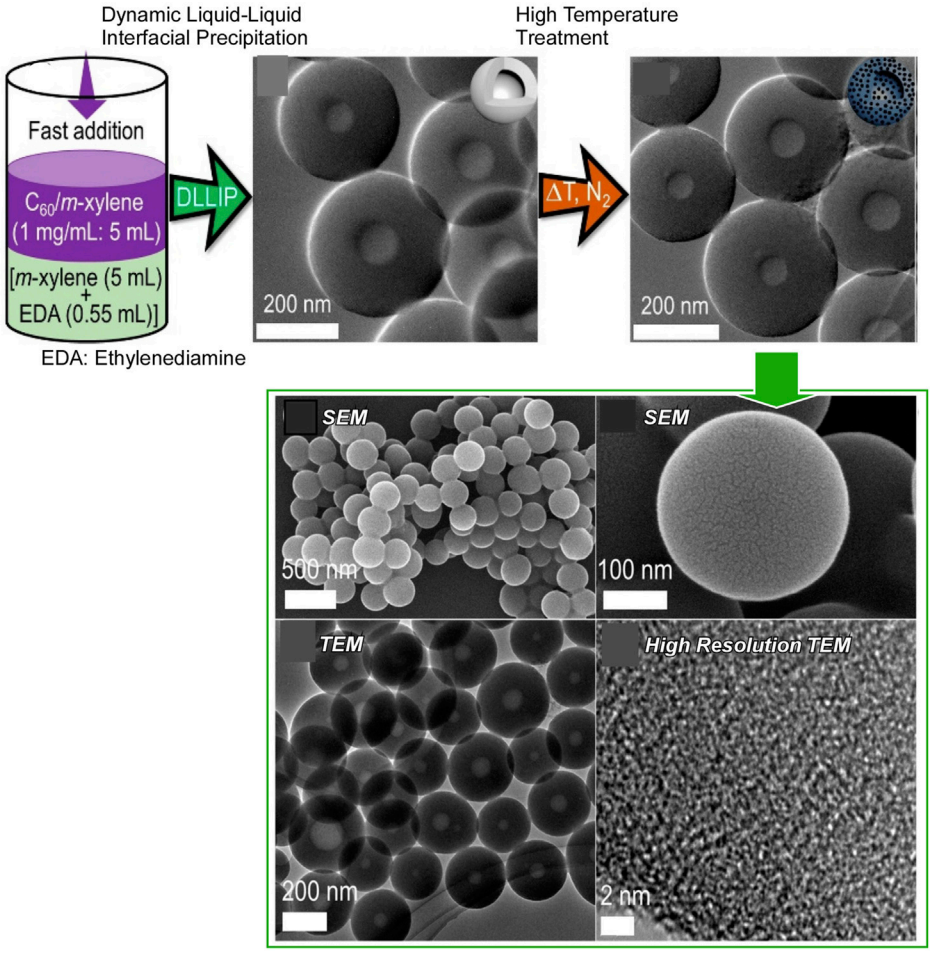

FIGURE 8
Self-assembled fullerene-ethylenediamine hollow spheres, which were carbonized at high temperatures to fabricate hollow carbon spheres. Reproduced under terms of the CC-BY license from Shrestha et al. (2023b) MDPI.

has an interconnected skeletal structure with a uniform pore distribution and narrow pore size distribution. The amorphous structure with graphitic carbon structure and partially developed mesoporous structures is induced by heat treatment due to the loss of crystallinity of C_{60}. The high surface area, large pore volume, and interconnected mesopore structure of the macaroni carbon tubes exhibit excellent electrochemical supercapacitance performance. Thus, the electrochemical performance of macaroni carbon tubes derived from a π-electron-rich carbon source was superior to materials based on graphene, carbon nanotubes, activated fullerenes, or nitrogen-doped activated fullerenes. Supercapacitor properties are higher than those of other well-known carbon materials. Tubular morphology with high electrochemical conductivity and interconnected nanoporous structures that facilitating electrode charge transport are key factors in superior electrochemical performance.

As seen in the examples above, the energy storage performance of supercapacitors is based on ultra-high specific surface area and rapid diffusion of electrolyte ions through interconnected channels in mesoporous structures. For this purpose, nanostructured hierarchical micro/mesoporous hollow structures are necessary for carbon materials. Shrestha and co-workers prepared self-assembled fullerene-ethylenediamine hollow spheres, which were carbonized at high temperatures to fabricate hollow carbon spheres (Figure 8) (Shrestha et al., 2023b). The fullerene-ethylenediamine hollow spheres were first prepared under ambient temperature conditions using the dynamic liquid-liquid interfacial deposition method. The fullerene-ethylenediamine hollow spheres had an average outer diameter of 290 nm, an inner diameter of 65 nm, and a thickness of 225 nm. This object was carbonized at high temperatures (700, 900, 1,100°C). Nanoporous hollow carbon spheres with large surface area and large pore volume were obtained depending on the processing temperature (Table 2). In particular, the carbon material obtained by carbonization at 900°C showed optimal structural characteristics, including well-developed porosity, interconnected pore structure, and large surface area. It showed remarkable electrochemical electric double-layer capacitance properties in 1 M sulfuric acid solution. Figure 9A shows the CV profiles of the reference FE-HS sample and the carbonized samples FE-HS_700, FE-HS_900, and FE-HS_1100. Here again, all the electrodes exhibit quasi-rectangular CV curves demonstrating EDLC behavior. Note that a minor redox peak at 0.5 V (oxidation) and 0.4 V (reduction) with minor intensity can be attributed to the oxygen

TABLE 2 Surface textural properties (surface area, pore volume and pore size) of the fullerene C60-ethyelendiamine hollow spheres (FE-HS), and the derived porous carbons obtained by high temperature carbonization of FE-HS (700°C–1,100°C) under the nitrogen gas atmosphere[a]. Reproduced under terms of the CC-BY license from Shrestha et al. (2023b) MDPI.

Sample	*SSA* (m^2 g^{-1})	S_{micro} (m^2 g^{-1})	S_{meso} (m^2 g^{-1})	V_p (cm^3 g^{-1})	V_{micro} (cm^3 g^{-1})	W_p (nm)	D_p (nm)
FE-HS	94.2	42.4	51.8	0.530	0.154	---	---
FE-HS_700	612.9	499.4	113.5	0.925	0.350	0.299	3.89
FE-HS_900	1,616.5	1,504.3	112.2	1.295	0.655	0.262	3.89
FE-HS_1100	1,439.3	1,264.2	175.1	1.346	0.630	0.274	3.90

[a]*SSA*, specific surface area; S_{micro}, surface area contributed from micropores; S_{meso}, surface area of mesopores; V_p, total pore volume; V_{micro}, micropore volume; W_p, micropore size (average half pore width); D_p, mesopore size (average pore diameter).

and nitrogen surface functionalities. In line with the porosity properties, the FE-HS_900 electrode delivered the highest total integral current among all the electrodes suggesting micropore-driven enhanced energy storage performance (Table 2). Due to a lack of porosity the reference sample FE-HS has the lowest integral current collection (Figure 9A) indicating its weak energy storage capacity. The specific surface area of the FE-HS_700 sample is significantly higher than that of FE-HS (Table 2). However, there is not much difference in the total current collection. The FE-HS_700 sample is a fullerene-EDA complex with lower conductivity compared to higher-temperature carbonized samples FE-HS_900 and FE-HS_1100. The CV recorded at different scan rates from 5 to 50 mV s^{-1} for FE-HS_900 and FE-HS_1100 electrodes show a sustain in the quasi-rectangular shape (Figures 9B, C), signifying quick electrolyte ion diffusion to the electrode surface promoted by the hierarchical micro/mesopore architectures. Figure 9D compares the GCD profiles at a fixed current density of 1 A g^{-1}, which, as revealed by the CV measurements, shows that the FE-HS_900 sample, due to the optimal surface area, shows the longest discharge time, inferring the highest energy storage capacity. The FE-HS and FE-HS_700 have low C_s of 73 and 81 F g^{-1}, respectively. On the other hand, FE-HS_900 and FE-HS_1100 exhibit much higher values of 293 and 283 F g^{-1} at 1 A g^{-1}, respectively. The GCD profiles vs. current densities for the optimal sample (Figure 9E) show the retention of a quasi-rectangular shape even at a high current density of 20 A g^{-1}. The C_s vs. current density plots (Figure 9F) reveal that the rate performances of the FE-HS_900 and FE-HS_1100 electrodes are also good, providing good specific capacitances respectively of 152 F g^{-1} (51.8%) and 147 F g^{-1} (51.9%) at the current rate of 20 A g^{-1}.

The high-performing electrode materials in the three-electrode systems (FE-HS_900 and FE-HS_1100) were considered for the supercapacitor device performance. Figure 10A shows CV profiles of the symmetric cells at a fixed scan rate of 5 mV s^{-1}. Perfect rectangular shapes of the CV curves confirm the EDLC charge storage behavior of the cell. The total integral current in the CV curves of FE-HS_900 and FE-HS_1100 suggest that both devices have a similar energy storage capacity. Figure 10B shows the CV curves of FE-HS_900 cell at different scan rates from 5 to 50 mV s^{-1}. The shape of the CV curve is sustained to its original rectangular shape even at a high scan rate of 50 mV s^{-1}. This infers a fast electrolyte ion diffusion, which is promoted by the presence of mesoporous channels with interconnected pore structures. Figures 10C–E shows the GCD profiles. Similar discharge times of both cells indicate similar energy storage capacities (Figure 10C). Fast electrolyte ion diffusion is seen in the GCD profiles at a higher current density of 10 A g^{-1} (Figures 10D, E). The specific capacitances of the symmetric cells are found to be 164 F g^{-1} (FE-HS_900) and 167 F g^{-1} (FE-HS_1100) at a current density of 1 A g^{-1} (Figure 10F), followed by a good rate performance (50% capacitance retention) at 10 A g^{-1}. Both systems showed an outstanding cycling life of 96% without substantial losses in columbic efficiency (98%) after 10,000 repeated charging/discharging cycles (Figure 10G). Figure 10H shows Nyquist plots from the electrochemical impedance spectroscopy (EIS) measurements. The semi-circular behavior in the high-frequency region with a ~45° slope in the low-frequency region implies charge transfer resistance and Warburg impedance. This phenomenon is common in hetero-atoms (oxygen and nitrogen) holding porous carbon materials. Figure 10I summarizes the energy density performance of the symmetric supercapacitors. The devices supplied a specific energy and specific power of 7.44 Wh $kg^{-1}$and 0.57 kW kg^{-1} (FE-HS_900) and 10.2 Wh kg^{-1} and 0.78 kW kg^{-1} (FE-HS_1100). These results indicate that carbon materials from the self-assembled fullerene-ethylenediamine hollow sphere have excellent energy storage performance as supercapacitors. Because of the simple preparation procedure, there is also great potential for scalable fabrication of carbon materials for supercapacitor applications.

As a new carbon material, fullerene C_{60} microbelt was prepared using the liquid-liquid interface precipitation method (Figure 11) (Tang et al., 2017). First, supramolecularly assembled structures of quasi-two-dimensional microbelt with a high aspect ratio of fullerene C_{60} were prepared at room temperature at the liquid-liquid interface of a carbon disulfide solution of fullerene C_{60} and isopropyl alcohol. The length of the synthesized fullerene C_{60} microbelt could be controlled by the synthesis conditions. Pseudo-2D mesoporous carbon microbelts were obtained by heat treatment of C_{60} microbelts at 900°C and 2000°C. At 900°C, the C_{60} microbelts were converted to an amorphous carbon structure. On the other hand, heat treatment at 2,000°C resulted in the formation of a graphite structure with densely packed graphene layers. In particular, microbelts heat-treated at 900°C had a high surface area, high pore volume, and a strong mesoporous framework developed. These structural characteristics resulted in excellent electrochemical supercapacitor performance. The carbon belts exhibited super-cycle stability: no capacity loss was observed after 10,000 charge-discharge cycles. These results suggest that quasi-two-

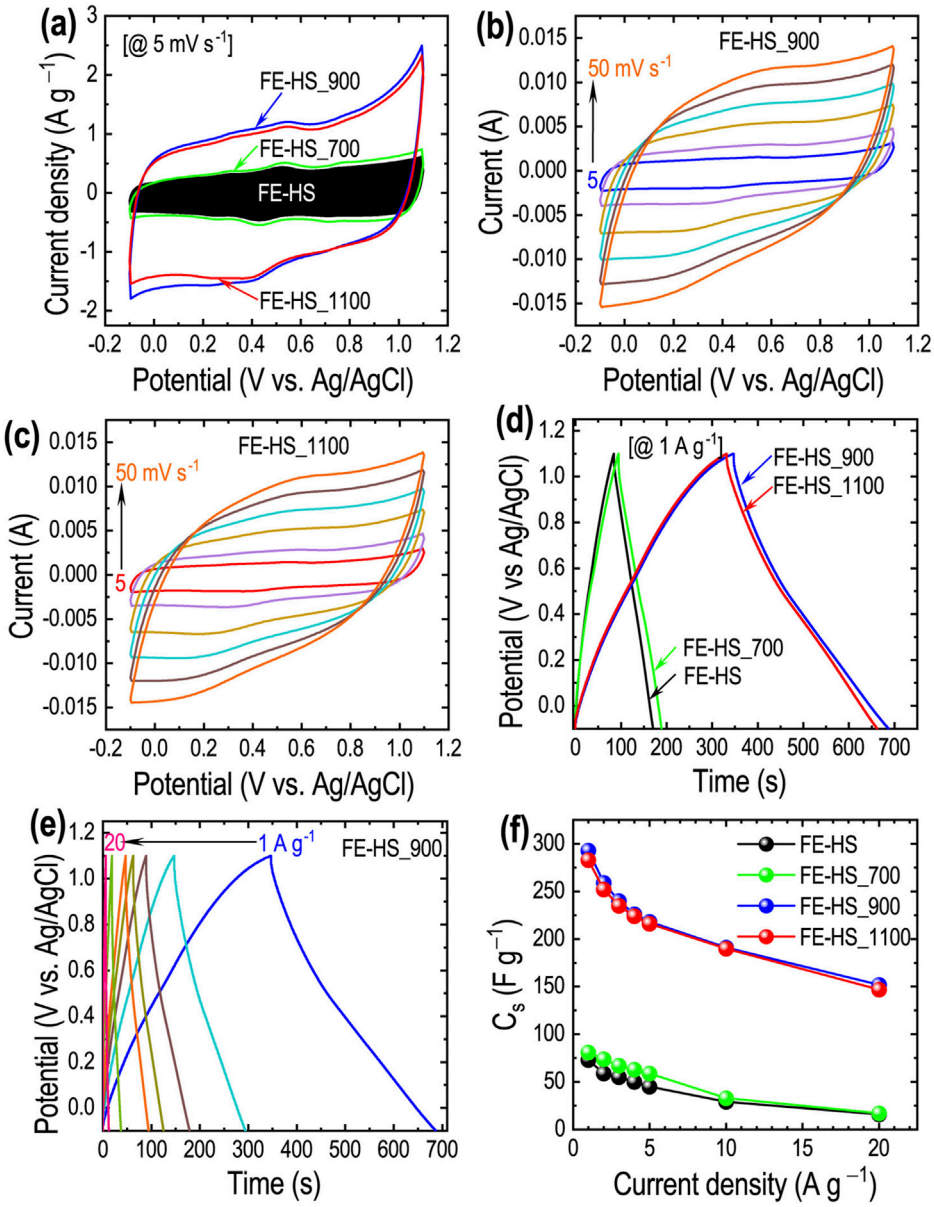

FIGURE 9
Electrochemical supercapacitance performance of fullerene-ethylenediamine hollow spheres derived nanoporous carbon materials. **(A)** Comparison of the CV curves a fixed scan rate of 5 mV s^{-1}, **(B,C)** CV profiles at different sweep for the samples carbonized at 900°C and 1,100°C, **(D)** comparison of GCD profiles at 1 A g^{-1} current density, **(E)** GCD profiles vs. current density for the electrode with optimal surface textural properties, and **(F)** calculated specific capacitances of all the electrodes at different current density from 1 to 20 Ag^{-1}. Reproduced under terms of the CC-BY license from Shrestha et al. (2023b) MDPI.

dimensional mesoporous carbon microbelts derived from π-electron-rich fullerene C_{60} crystals are promising materials for electrochemical supercapacitor applications.

C_{70} is also used as a fullerene carbon source. Mesoporous crystalline fullerene C_{70} microtubes were first prepared by supramolecular assembly. This structure was directly converted into mesoporous graphitic carbon microtubes by heat treatment at 2,000°C (Figure 12) (Bairi et al., 2016b). The original one-dimensional tubular morphology was retained during this carbonization process. The walls of the resulting graphitic carbon microtubes were composed of ordered conjugated sp^2 carbons with a strong mesoporous framework structure. In other words, mesopores have developed on the tube surface, and the crystalline C_{70} has been completely transformed into highly graphitized carbon. Cyclic voltammetry and chronopotentiometry measurements show that this carbon material exhibits high specific capacitance. These results indicate that fullerene C_{70} is a promising source of π-electron carbon; mesoporous graphitic carbon microtubes derived from C_{70} are also promising electrode materials for high-performance electrochemical supercapacitor applications.

Other forms of carbon materials created from C_{70} are also useful in energy storage applications. Figure 13 shows that 3D mesoporous

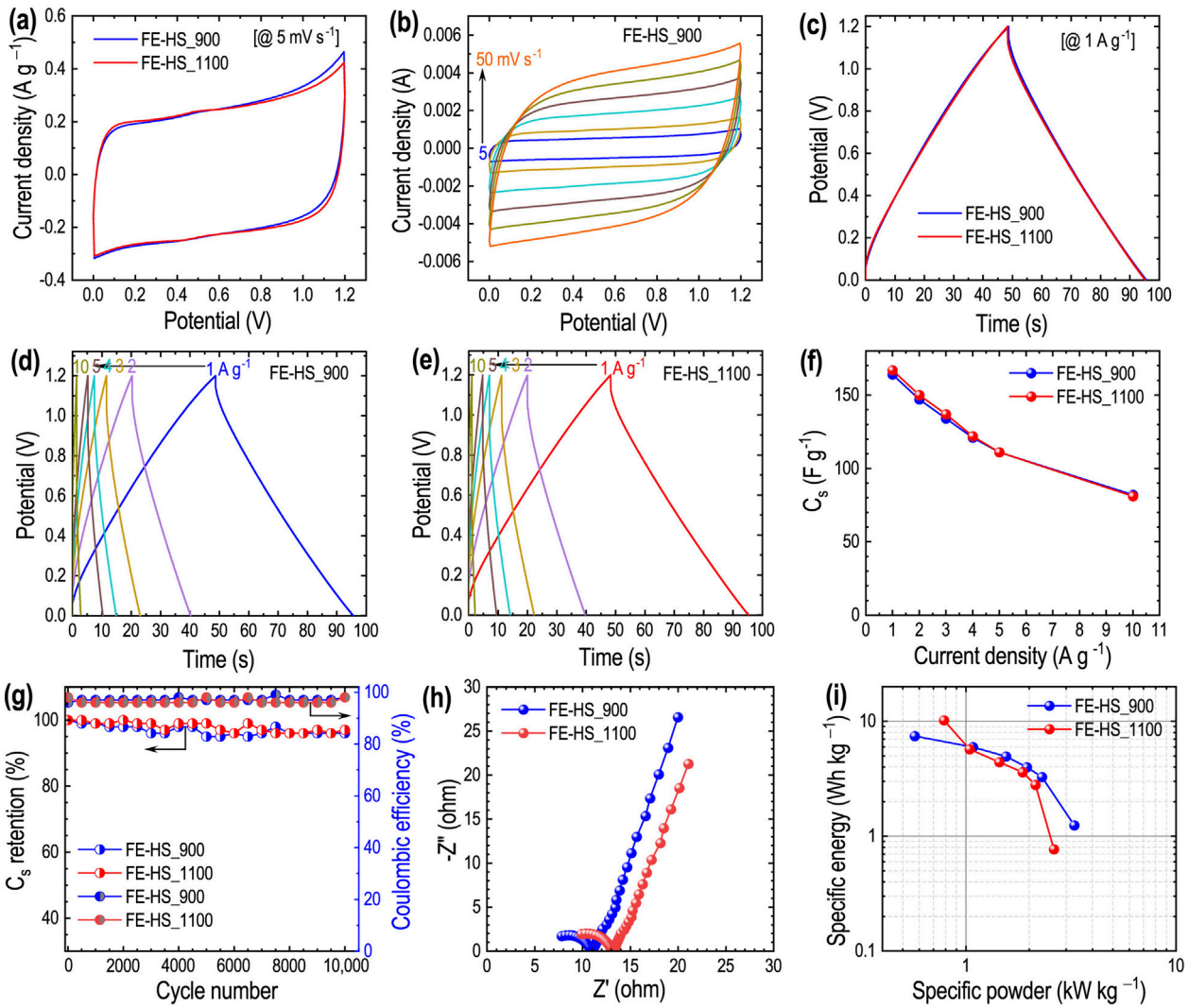

FIGURE 10
Supercapacitance performance of the assembled symmetric cells prepared using fullerene-ethylenediamine hollow spheres derived nanoporous carbon materials carbonized at 900°C and 1,100°C. **(A)** CV curves of the cells recorded at 5 mVs^{-1} **(B)** CV curves at different scan rates, **(C)** GCD curves at 1 A g^{-1}, **(D–E)** GCD profiles vs. current density; **(F)** calculated specific capacitance, **(G)** cycle performance and coulombic efficiency; **(H)** Nyquist plots, and **(I)** Ragon plots of the symmetric supercapacitors. Reproduced under terms of the CC-BY license from Shrestha et al. (2023b) MDPI.

crystalline fullerene C_{70} cubes (MCFC) can be fabricated and thermally converted to mesoporous carbon while retaining their original cubic morphology (Bairi et al., 2019). Mesoporous crystalline fullerene C_{70} cubes are treated by high-temperature heat treatment at 900°C under a nitrogen gas atmosphere to obtain mesoporous carbon cubes (MCFC-900) with amorphous structure. After the carbonization, the original cubic morphology is retained in the 900°C carbon. Clear 3D cubic morphology and high porous structure are confirmed by TEM in the MCFC-900 sample. High-resolution TEM observations revealed an amorphous carbon structure (Figure 13). The synthesized mesoporous carbon cubes exhibit excellent electrochemical capacitive properties. Figure 14A compares the CV curves of MCFC and MCFC-900, i.e., before and after heat treatments at a fixed scan rate of 5 mV s^{-1}. The total current collection of the MCFC-900 sample is much higher than that of the starting material MCFC. This suggests the higher energy storage capacity of MCFC-900 compared to the MCFC. The CV curves vs. scan rate profiles of MCFC-900 (Figure 14B) reveal rapid current response and show a quasi-rectangular shape at low scan rates, appearing to be a characteristic of EDLCs. The CV profile departs from a rectangular shape with increasing scan rates due to oxygenated functional groups on the carbon surface. Figure 14C shows the GCD profiles of the MCFC-900 recorded at different current densities. The triangular charge-discharge profile with a long discharging tail confirms that the EDLC charge storage has a large capacitance. A high specific capacitance of 205 F g^{-1} was calculated at a current density of 1 A g^{-1} followed by a very high retention of specific capacitance (56.0%) at a high current density of 20 A g^{-1} demonstrating the high-rate performance of MCFC-900 (Figure 14D). Furthermore, after 10,000 cycles, no decrease in specific capacitance was observed (Bairi et al., 2019). This novel mesoporous carbon with cubic morphology could be a potential

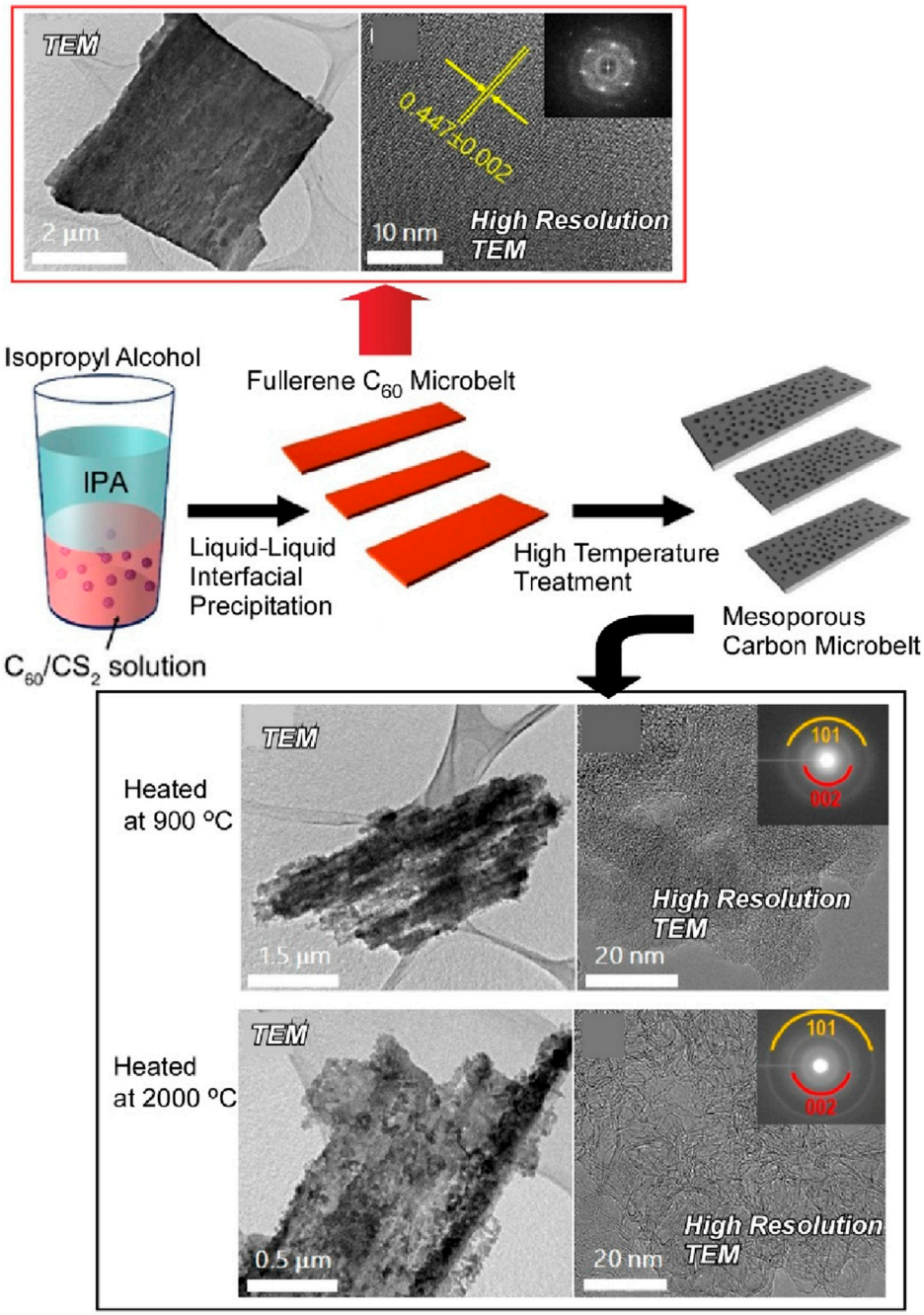

FIGURE 11
Preparation of fullerene C_{60} microbelt using the liquid-liquid interface precipitation method and mesoporous carbon microbelt by heat treatment at 900°C and 2,000°C. Reprinted with permission from Tang et al. (2017) American Chemical Society.

electrode material for high-rate performance supercapacitors applications.

We have summarized the electrochemical energy storage performance of various porous carbon materials synthesized from natural biomass and synthetic carbon precursors (Table 3). It can be seen that in an aqueous electrolyte system (acidic, alkaline, and neutral medium), the specific capacitance of a single electrode in the three-electrode cell setup largely depends on the surface textural properties, pore size distribution, conductivity wet, stability, and surface functionality of the electrode materials. The overall energy storage capacity of supramolecular fullerene assemblies-derived hierarchically porous carbon materials is higher or comparable to the ultra-high surface area of microporous and nanoporous biomass carbon materials. For example, porous carbon tubes obtained by the high-temperature carbonization of macaroni fullerene crystals achieved an outstanding specific capacitance of 422 F g^{-1} at a current density of 1 A g^{-1} due to hierarchical pores with micro- and mesopore architectures and interconnected mesopore structures, which enhances the ion diffusion to the electrode surface. On the other hand, compared to macaroni fullerene

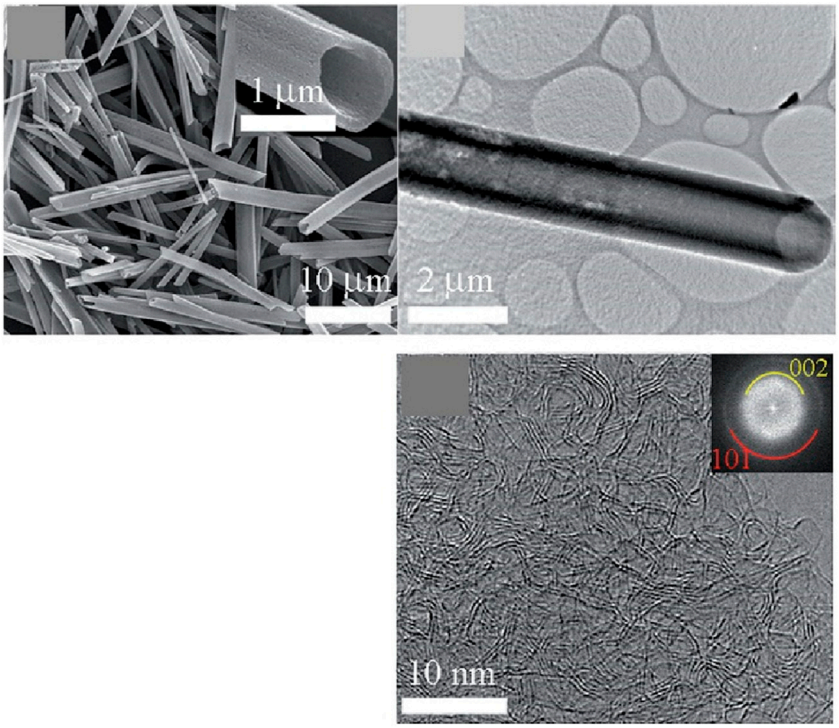

FIGURE 12
Images of mesoporous graphitic carbon microtubes from mesoporous crystalline fullerene C_{70} microtubes by heat treatment at 2000°C. Reproduced under terms of the CC-BY license from Bairi et al. (2016b) Royal Society of Chemistry.

crystals-derived carbon tubes, the Houttuynia biomass-derived carbon material achieved even higher specific capacitance (473 F g^{-1} at 1 A g^{-1}) due to ultrahigh surface area (2090 m^2g^{-1}) and 3D hierarchically porous high nitrogen-doped carbon nanostructure (~8 wt%) (Shang et al., 2020). The specific capacitance was further improved with the carbon nanosheets obtained from Prosopis Juliflora wood carbon waste blocks. An outstanding electrochemical performance with a specific capacitance of 588 F g^{-1} at 0.5 A g^{-1} with excellent stability (retention 92.5% after 6,000 cycles) was found in 6 M KOH electrolyte (Selvaraj et al., 2021), which was caused due to ultra-high specific surface area (2,943 m^2g^{-1}), and ample pore volume (1.83 cm^3g^{-1}) followed by a rational micro/meso/macro pore size distributed in the carbon flakes like 2D nanosheets.

We have also compared the symmetric cell performances of carbon materials prepared from both carbon sources (Table 4). Most electrochemical performance studies revealed that the porous carbon materials prepared from biomass carbon precursors deliver energy density in the range of 5–60 Wh/kg depending on the surface area, pore size distribution, morphology of the carbon particles, surface functionality, wetting properties, etc. Microporous carbon materials with irregular shape particle type morphology show a high specific capacitance in the tree-electrode cell setup, especially at low current density. However, they offer a limited energy density in the symmetric cells, generally in the range of 5–10 Wh/kg, due to inappropriate pore sizes to promote ion diffusion, surface functionality to improve the wetting, and low conductivity for charge transfer at the electrode surface. For example, a symmetric cell prepared using the porous carbon prepared from Sichuan pepper achieved an energy density of 4.2 Wh/kg at a power density of 0.25 kW/kg. Compared to Sichuan pepper-derived carbon, nitrogen-doped 3D hierarchically porous honeycomb-like nanostructured carbon materials prepared from Houttuynia biomass showed superior energy density performance in the symmetric cell, offering a higher energy density of 15.99 Wh/kg at 0.5 kW/kg of power density. The energy density performance could be improved with the 3D hierarchical porous nanosheet carbon electrode obtained from Prosopis Juliflora carbon. The symmetric cell delivered a high energy density of 56.7 Wh/kg at a power density of 0.78 kW/kg in aqueous electrolyte (1 M Na_2SO_4) due to ultrahigh surface area, enhanced degree of graphitization, surface functionalities (nitrogen- and oxygen doping: contact angle ~32° showing good wetting properties), and pore structure/volume. Compared to the symmetric cells prepared using biomass carbon materials, the cell prepared with the fullerene crystal-derived carbon materials offers lower energy density in the range of ~10 Wh/kg, which is due to the lack of surface functionalities as the starting material the self-assembled fullerene crystals are purely made of fullerene molecules without any surface functionalities. However, it could sustain higher power density, an intrinsic property of supercapacitors, compared to biomass carbons. To further enhance the energy performance of the fullerene-derived porous carbons, a higher degree of graphitization and hetero-atom doping is essential to improve the conductivity and wetting of the electrode surface. With multi-dimensional morphologies of the fullerene assemblies, producing functional hierarchical porous carbons with high-energy performance supercapacitors would be advantageous.

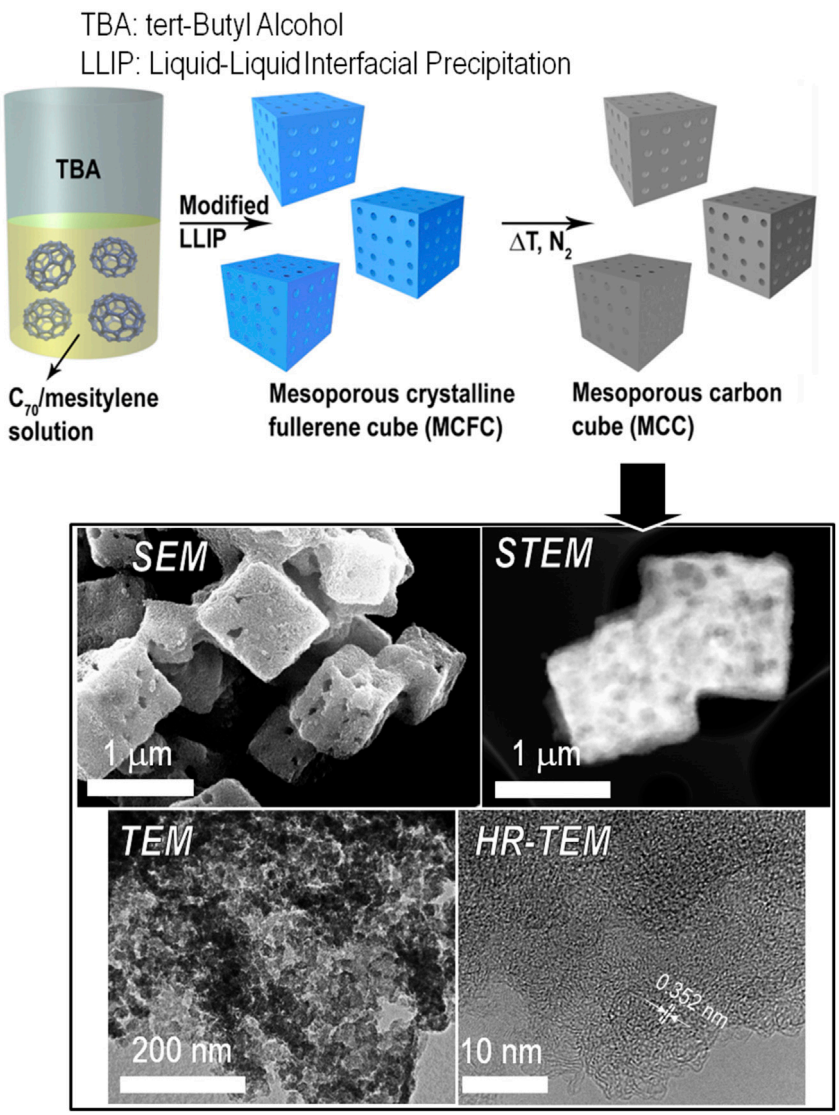

FIGURE 13
Preparation of mesoporous carbon cubes from mesoporous crystalline fullerene C_{70} cubes through heat treatment at high temperatures (900°C and 2000°C). Reprinted with permission from Bairi et al. (2019) Royal Society of Chemistry.

4 Summary and perspectives: biomass vs. fullerene

For summary and perspectives, examples of porous carbon materials prepared from biomass sources and through fullerene assemblies and their applications in supercapacitors are compared from viewpoints of advantages, disadvantages, future necessity, and so on.

Over the past few decades, a wide range of nanostructured materials, including nanoporous materials, have been developed as potential electrode materials for advanced supercapacitors. Most materials explored include conductive polymers, metallic nanoparticles, metal oxides, sulfides, selenides, and hydroxides. Indeed, these pseudocapacitor electrode materials undergo Faradic reaction at the electrode surface and exhibit superior specific capacitance compared to the EDLC. However, due to the low electrical conductivity, environmental harmfulness, and poor cycling stability, these materials are unsuitable for an environmentally safe society and thus are unsuccessful commercially. Therefore, massive interest has been paid to carbonaceous materials because of low-cost production, good electrical conductivity, excellent thermochemical stability, surface functionality, and environmental friendliness. Several carbonaceous materials, including elite carbon materials such as fullerene, carbon nanotubes, graphene, carbon aerogel and ordered porous carbons, carbon nanohorns, and so on, have been widely explored in energy storage systems. Porous carbon materials fabricated from natural biomass precursors have become a focus in energy storage, energy conversion, sensing, separation, and purification because these precursors are

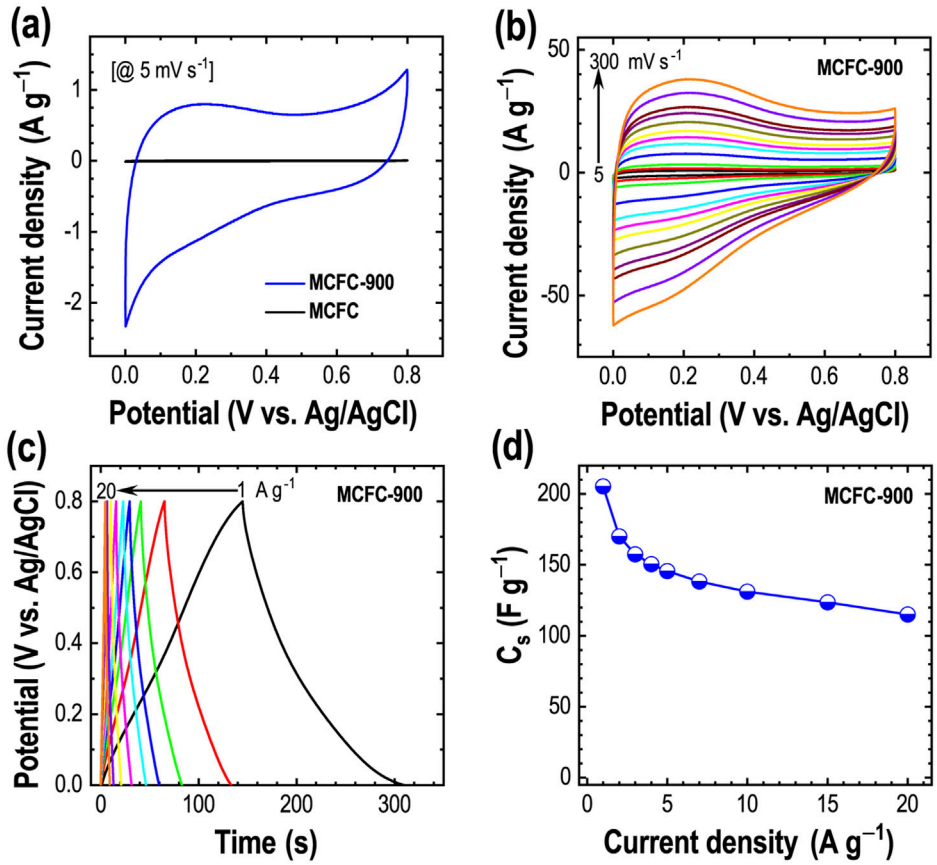

FIGURE 14
Supercapacitance performance of micro/mesoporous carbon cubes prepared by the direct carbonization of fullerene cubes at high temperature (900°C). **(A)** Comparison of CV curves for reference and carbonized sample at 5 mV s^{-1}, **(B)** CV response at higher scan rates up to 300 mV s^{-1}, **(C)** GCD profiles from 1 to 20 A g^{-1}, and **(D)** the corresponding specific capacitance of the carbonized samples showing the high-rate performance of the electrode. Reprinted with permission from Bairi et al. (2019) Royal Society of Chemistry.

sustainable, renewable precursors, and environmentally friendly. The fabrication process is relatively simple to make it suitable for large-scale production for commercialization.

As discussed in the previous sections, hierarchically porous carbon materials with a three-dimensional network structure, ultrahigh surface area, and well-defined pore structures are highly demanded in energy storage applications, and they can be fabricated from different synthetic or natural carbon sources. We described the self-assembled fullerene crystals as excellent π-electron-rich synthetic carbon sources for producing high surface area nanoporous carbons with well-defined pore structures. Fullerene is advantageous over biomass because of its several intriguing properties that enable the fabrication of porous carbons with desired porosity and interconnectivity among the pore architectures. Furthermore, fullerene molecules (C_{60} and C_{70}) function as unique functional building blocks, forming several supramolecular self-assemblies through the π-stacking interactions, enabling the facile fabrication of shape- and size-controlled fullerene crystals. One can fabricate fullerene assemblies from 0D (spheres), 1D (rods and tubes), 2D (sheet and disks) to 3D (cubes), hollow structures with tunable thickness, and hierarchical superstructures such as fullerene cubic shape core with nanorods coming out of the cube surface. Fullerene self-assemblies and the derived porous graphitic carbon materials have been well explored in gas sensing, especially volatile organic compounds. They are sensitive to toxic aromatic vapors due to strong π-π interaction promoted by the diffusion of the guest in the mesoporous structure, demonstrating its potential impact in the environment.

Interestingly, all these fullerene nanomaterials can be converted into nanoporous carbon materials upon high-temperature carbonization without losing the morphology. Thus, using fullerene crystals as the carbon source, one can quickly and efficiently fabricate nanoporous carbons with well-defined shapes, which cannot be obtained by carbonization or activation of biomass. Furthermore, fullerene crystals derived porous carbons have a higher graphitic degree compared to the biomass carbons and exhibit hierarchical pore architectures composed of both micro- and mesopore structures with interconnected pore structures, which is not so common in the activated carbons obtained from biomass. One can use fullerene crystals as the carbon source to prepare ultrahigh surface area nanoporous carbon by single-step direct carbonization without any activators. Temperature, heating ramp,

TABLE 3 Electrochemical supercapacitance performance (comparison of specific capacitances) of porous carbon materials prepared from different biomass carbon precursors and fullerene crystals.

Carbon precursors	Electrolyte	Current density (A g^{-1})	C_s (F g^{-1})	Ref.
Walnut shell ($KMnO_4$ activated)	6 M KOH	0.5	380	Zhang et al. (2023)
Lapsi seed ($ZnCl_2$ activated)	1 M H_2SO_4	1	284	Shrestha et al. (2020b)
Date seed (KOH activated)	1 M H_2SO_4	1	386	Shrestha et al. (2022b)
Barro seed stone ($ZnCl_2$ activated)	1 M H_2SO_4	1	319	Gnawali et al. (2023a)
Konpeito-like fullerene crystals	1 M H_2SO_4	1	115	Shrestha et al. (2016)
Mesoporous carbon tubes	1 M H_2SO_4	1	422	Maji et al. (2021b)
Carbon hollow spheres	1 M H_2SO_4	1	293	Shrestha et al. (2023b)
C_{60} microbelts	1 M H_2SO_4	1	290	Tang et al. (2017)
Fullerene microtubes	1 M H_2SO_4	0.5	184	Bairi et al. (2016b)
Fullerene cubes	1 M H_2SO_4	1	205	Bairi et al. (2019)
Harro seed stone ($ZnCl_2$ activated)	1 M H_2SO_4	1	328	Gnawali et al. (2023b)
Apple-pomace (K_2FeO_4 activated)	6 M KOH	0.5	360	Zhang et al. (2022)
Tasmanian Blue Gum (KOH activated)	1 M KOH	1	212	Prasankumar et al. (2022)
Lotus leaf (KOH activated)	6 M KOH	0.5	425	Liu et al. (2021b)
Corn husk (K_2CO_3 activated)	0.5 M H_2SO_4	0.25	225	Lobato-peralta et al. (2023)
American ginseng waste residue	6 M KOH	0.1	268	Tu et al. (2023)
Coconut shell (KOH activated)	0.5 M Na_2SO_4	1	397	Wang et al. (2022)
Rotten wood ($ZnCl_2$ activated)	6 M KOH	1	350	Wang et al. (2023)
Lotus seed ($ZnCl_2$ activated)	1 M H_2SO_4	1	272	Shrestha et al. (2020c)
Washnut seed (KOH activated)	1 M H_2SO_4	1	288	Shrestha et al. (2021b)
Washnut seed ($ZnCl_2$ activated)	1 M H_2SO_4	1	225	Shrestha et al. (2020d)
Jackfruit seed ($ZnCl_2$ activated)	1 M H_2SO_4	1	261	Chaudhary et al. (2020)
Pine Sawdust (CO_2 activated)	6 M KOH	1	225	Gao et al. (2020)
Citrus bergamia peels	6 M KOH	0.1	289	Gehrke et al. (2021)
Prosopis juliflora wood (KOH activated)	6 M KOH	0.5	588	Selvaraj et al. (2021)
Corncob (KOH activated)	6 M KOH	0.5	382	Song et al. (2020)
Cotton fiber (NaOH activated)	3 M KOH	0.3	222	Liu et al. (2016)
Cottonseed hull (KOH activated)	6 M KOH	0.5	304	Jiang et al. (2018)
Bio-decomposited product	6 M KOH	0.05	209	Zhu et al. (2018)
Lignocellulose carbon	1 M NaCl	1	172	Lu et al. (2020)
Biomass-derived lignin	6 M KOH	0.5	348	Cao et al. (2021)
Kraft lignin (CO_2 activated)	6 M KOH	0.1	155	Schlee et al. (2019)
Salvia splendens (NaCl activated)	6 M KOH	1	294	Liu et al. (2018)
Yeast (Na_2SiO_3 activated)	6 M KOH	0.5	313	Tian et al. (2022)
Wood sawdust (KOH activated)	6 M KOH	0.5	225	Huang et al. (2016)
Wood	1 M H_2SO_4	0.5	260	Chen et al. (2020)
Houttuynia biomass (KOH activated)	6 M KOH	1	473	Shang et al. (2020)

TABLE 4 Comparison of the energy density of symmetric supercapacitor cells prepared using porous carbon materials obtained from different carbon sources (biomass and fullerene).

Carbon precursors	Energy density (W h/kg)	Power density (kW/kg)	Ref
Fullerene-ethylenediamine hollow carbons	10.2	0.78	Shrestha et al. (2023b)
Prosopis juliflora	56.7	0.24	Selvaraj et al. (2021)
Houttuynia biomass	15.9	0.5	Shang et al. (2020)
Bamboo-derived carbon	5.4	0.5	Abbas et al. (2022)
Coal-tar pitch	6.45	0.48	Jiang et al. (2022b)
Chitosan	10.46	0.5	Chen et al. (2021c)
Sichuan pepper	4.2	0.25	Zhang et al. (2019)
Rice husk	16.7	0.4	Arkhipova et al. (2022)
Baobab fruit shell	20.86	0.4	Mohammed et al. (2019)
Peanut shells	22.2	0.31	Liang et al. (2023)
Syzygium cumini fruit shells	27.22	0.2	Vinayagam et al. (2020)
Polyalthia longifolia seeds	27.5	0.49	Srinivasan et al. (2019)
Keratin	32	0.32	Sinha et al. (2020)
Eulaliopsis binata straw	40.14	0.27	Liu et al. (2023b)
N-doped rice straw	48.9	0.75	Charoensook et al. (2021)
Onion like fullerene	10.6	0.10	Mohapatra et al. (2019)

and hold time are the only parameters to tune the porosity. One can keep the pentagon properties of the fullerene molecule depending on the requirement by subtly tuning the temperature.

Despite the several advantages of fullerene crystals as a carbon source, commercial fullerenes are expensive. Scale-up synthesis is essential for commercial and practical applications of porous carbon materials, which would be extremely expensive with the fullerenes. For the scale-up production of carbon materials on an industrial scale, biomass is beneficial. It is a natural and sustainable carbon source. Therefore, most of the commercial carbons are produced from biowaste, such as coconut shells, sugarcane baggage, rice husks, etc. The carbon source itself is cost-free. It's only the processing cost of the biomass carbon. However, the carbon materials obtained by the high-temperature heat treatment of the biomass result in the formation of non-porous or low surface area carbon with poorly developed pore structures. A significant amount of chemical activating agents is required to produce high-porosity biomass carbons. Furthermore, chemically activated biomass carbon generally forms mere micropores, which is not beneficial in energy storage supercapacitor applications. For high-performance energy storage applications, porous carbon with micro- and mesopore structures is required. Mesopores, especially interconnected mesopores, serve as the channels for the electrolyte ion transfer from the solution to the electrode surface and enhance the rate and cycle performance of the supercapacitors. Another technical issue with biomass is its complex composition and compositional variation, resulting in different surface area carbons from the same biomass. Unlike the template (soft- or hard-template) synthesis of porous carbon, nanopore engineering is challenging with biomass carbons. A deeper fundamental study to tailor the pore size is required to produce hierarchically porous carbon materials from the sustainable biomass carbon source on the industrial scale at a low cost, which will be an asset in designing practical high-performance supercapacitors devices. As discussed in the symmetric cell, the performance of carbon materials prepared from different sources could deliver limited energy density, which is yet far from fulfilling society's energy demand. Therefore, to enhance the energy density performances of biomass and fullerene-derived porous carbons, the synthesis of hierarchical porous architectures with interconnected micro-, meso-, and macropores with hetero-atom doping with a high degree of graphitization can be regarded as the strategic ideal material design. Nevertheless, choosing the appropriate biomass and approach to synthesize hierarchical porous carbon with outstanding electrochemical properties for high-performance supercapacitors is challenging. Combining biomass- and fullerene-derived materials may exhibit synergy to improve properties and capacitance performance. Furthermore, growing fullerene assemblies in the meso- and macroporous honeycombs or channels of the biomass carbons and consequent activation/carbonization may enhance the textural properties and energy density.

This short review concisely shows a variety of nanoarchitectonics approaches for nanostructured carbon materials for the same purpose as supercapacitors. Although these approaches are based on totally different sources, biomass and fullerene, the obtained properties and further demanded requirements have common features. On the other hand, these sources have different advantages and disadvantages. Nanoarchitectonics approaches are versatile for many materials, but its efficient usages require deeper considerations depending on the materials selection.

Author contributions

LS: Writing–review and editing, Writing–original draft, Visualization, Data curation. KA: Writing–review and editing, Validation, Supervision, Resources, Funding acquisition, Data curation, Conceptualization.

Funding

The author(s) declare that financial support was received for the research, authorship, and/or publication of this article. This study was partially supported by Japan Society for the Promotion of Science KAKENHI (Grant Numbers JP20H00392 and JP23H05459).

Conflict of interest

The authors declare that the research was conducted in the absence of any commercial or financial relationships that could be construed as a potential conflict of interest.

Publisher's note

References

Abbas, S. C., Lin, C., Hua, Z., Deng, Q., Huang, H., Ni, Y., et al. (2022). Bamboo-derived carbon material inherently doped with SiC and nitrogen for flexible supercapacitors. *Chem. Eng. J.* 433, 133738. doi:10.1016/j.cej.2021.133738

Aono, M., and Ariga, K. (2016). The way to nanoarchitectonics and the way of nanoarchitectonics. *Adv. Mater.* 28, 989–992. doi:10.1002/adma.201502868

Ariga, K. (2021). Nanoarchitectonics: what's coming next after nanotechnology? *Nanoscale Horiz.* 6, 364–378. doi:10.1039/d0nh00680g

Ariga, K. (2023a). Liquid-liquid interfacial nanoarchitectonics. *Small* 20, 2305636. doi:10.1002/smll.202305636

Ariga, K. (2023b). Materials nanoarchitectonics: collaboration between chem, nano and mat. *Chem. Nano. Mat* 9, e202300120. doi:10.1002/cnma.202300120

Ariga, K. (2023c). Chemistry of materials nanoarchitectonics for two-dimensional films: Langmuir–Blodgett, layer-by-layer assembly, and newcomers. *Chem. Mater* 35, 5233–5254. doi:10.1021/acs.chemmater.3c01291

Ariga, K. (2024). Nanoarchitectonics: the method for everything in materials science. *Bull. Chem. Soc. Jpn.* 97, uoad001. doi:10.1093/bulcsj/uoad001

Ariga, K., and Fakhrullin, R. (2022). Materials nanoarchitectonics from atom to living cell: a method for everything. *Bull. Chem. Soc. Jpn.* 95, 774–795. doi:10.1246/bcsj.20220071

Ariga, K., Ji, Q., Nakanishi, W., Hill, J. P., and Aono, M. (2015). Nanoarchitectonics: a new materials horizon for nanotechnology. *Mater Horiz.* 2, 406–413. doi:10.1039/c5mh00012b

Ariga, K., Jia, X., Song, J., Hill, J. P., Leong, D. T., Jia, Y., et al. (2020). Nanoarchitectonics beyond self-assembly: challenges to create bio-like hierarchic organization. *Angew. Chem. Int. Ed.* 59, 15424–15446. doi:10.1002/anie.202000802

Ariga, K., Li, J., Fei, J., Ji, Q., and Hill, J. P. (2016). Nanoarchitectonics for dynamic functional materials from atomic-/molecular-level manipulation to macroscopic action. *Adv. Mater.* 28, 1251–1286. doi:10.1002/adma.201502545

Ariga, K., Lvov, Y., and Decher, G. (2022). There is still plenty of room for layer-by-layer assembly for constructing nanoarchitectonics-based materials and devices. *Phys. Chem. Chem. Phys.* 24, 4097–4115. doi:10.1039/d1cp04669a

Ariga, K., Nishikawa, M., Mori, T., Takeya, J., Shrestha, L. K., and Hill, J. P. (2019). Self-assembly as a key player for materials nanoarchitectonics. *Sci. Technol. Adv. Mater.* 20, 51–95. doi:10.1080/14686996.2018.1553108

Ariga, K., Song, J., and Kawakami, K. (2024). Layer-by-layer designer nanoarchitectonics for physical and chemical communications in functional materials. *Chem. Commun.* 60, 2152–2167. doi:10.1039/d3cc04952c

Arkhipova, E. A., Novotortsev, R. Y., Ivanov, A. S., Maslakov, K. I., and Savilov, S. V. (2022). Rice husk-derived activated carbon electrode in redox-active electrolyte-new approach for enhancing supercapacitor performance. *J. Energy Storage* 55, 105699. doi:10.1016/j.est.2022.105699

Azzaroni, O., Piccinini, E., Fenoy, G., Marmisollé, W., and Ariga, K. (2023). Field-effect transistors engineered via solution-based layer-by-layer nanoarchitectonics. *Nanotechnology* 34, 472001. doi:10.1088/1361-6528/acef26

Bairi, P., Maji, S., Hill, J. P., Kim, J. H., Ariga, K., and Shrestha, L. K. (2019). Mesoporous carbon cubes derived from fullerene crystals as a high rate performance electrode material for supercapacitors. *J. Mater Chem. A* 7, 12654–12660. doi:10.1039/c9ta00520j

Bairi, P., Minami, K., Hill, J. P., Ariga, K., and Shrestha, L. K. (2017). Intentional closing/opening of "hole-in-cube" fullerene crystals with microscopic recognition properties. *ACS Nano* 11, 7790–7796. doi:10.1021/acsnano.7b01569

Bairi, P., Minami, K., Nakanishi, W., Hill, J. P., Ariga, K., and Shrestha, L. K. (2016a). Hierarchically structured fullerene C_{70} cube for sensing volatile aromatic solvent vapors. *ACS Nano* 10, 6631–6637. doi:10.1021/acsnano.6b01544

Bairi, P., Shrestha, R. G., Hill, J. P., Nishimura, T., Ariga, K., and Shrestha, L. K. (2016b). Mesoporous graphitic carbon microtubes derived from fullerene C_{70} tubes as a high performance electrode material for advanced supercapacitors. *J. Mater Chem. A* 4, 13899–13906. doi:10.1039/c6ta04970b

Bhadra, B. N., Shrestha, L. K., and Ariga, K. (2022). Porous carbon nanoarchitectonics for the environment: detection and adsorption. *CrystEngComm.* 24, 6804–6824. doi:10.1039/d2ce00872f

Bogachuk, D., Girard, J., Tilala, S., Martineau, D., Narbey, S., Verma, A., et al. (2023). Nanoarchitectonics in fully printed perovskite solar cells with carbon-based electrodes. *Nanoscale* 15, 3130–3134. doi:10.1039/d2nr05856a

Cao, L., Huang, Y., Parakhonskiy, B., and Skirtach, A. G. (2022). Nanoarchitectonics beyond perfect order—not quite perfect but quite useful. *Nanoscale* 14, 15964–16002. doi:10.1039/d2nr02537j

Cao, M., Wang, Q., Cheng, W., Huan, S., Hu, Y., Niu, Z., et al. (2021). A novel strategy combining electrospraying and one-step carbonization for the preparation of ultralight honeycomb-like multilayered carbon from biomass-derived lignin. *Carbon* 179, 68–79. doi:10.1016/j.carbon.2021.03.063

Chaikittisilp, W., Yamauchi, Y., and Ariga, K. (2022). Material evolution with nanotechnology, nanoarchitectonics, and materials informatics: what will be the next paradigm shift in nanoporous materials? *Adv. Mater.* 34, 2107212. doi:10.1002/adma.202107212

Chapman, A., Eltekin, E., Kubota, M., Nagao, A., Bertsch, K., Macadre, A., et al. (2022). Achieving a carbon neutral future through advanced functional materials and technologies. *Bull. Chem. Soc. Jpn.* 95, 73–103. doi:10.1246/bcsj.20210323

Charoensook, K., Huang, C.-L., Tai, H.-C., Lanjapalli, V. K., Chiang, L.-M., Hosseini, S., et al. (2021). Preparation of porous nitrogen-doped activated carbon derived from rice straw for high-performance supercapacitor application. *J. Taiwan Inst. Chem. Eng.* 120, 246–256. doi:10.1016/j.jtice.2021.02.021

Chaudhary, R., Maji, S., Shrestha, R. G., Shrestha, R. L., Shrestha, T., Ariga, K., et al. (2020). Jackfruit seed-derived nanoporous carbons as the electrode material for supercapacitors. *C J Carbon Res* 6, 73. doi:10.3390/c6040073

Chen, G., Bhadra, B. N., Sutrisno, L., Shrestha, L. K., and Ariga, K. (2022a). Fullerene rosette: two-dimensional interactive nanoarchitectonics and selective vapor sensing. *Int. J. Mol. Sci.* 23, 5454. doi:10.3390/ijms23105454

Chen, G., Sciortino, F., and Ariga, K. (2021a). Atomic nanoarchitectonics for catalysis. *Adv. Mater. Interfaces* 8, 2001395. doi:10.1002/admi.202001395

Chen, G., Sciortino, F., Takeyasu, K., Nakamura, J., Hill, J. P., Shrestha, L. K., et al. (2022c). Hollow spherical fullerene obtained by kinetically controlled liquid-liquid interfacial precipitation. *Chem. – An Asian J.* 17, e202200756. doi:10.1002/asia.202200756

Chen, G., Shrestha, L. K., and Ariga, K. (2021b). Zero-to-two nanoarchitectonics: fabrication of two-dimensional materials from zero-dimensional fullerene. *Molecules* 26, 4636. doi:10.3390/molecules26154636

Chen, G., Singh, S. K., Takeyasu, K., Hill, J. P., Nakamura, J., and Ariga, K. (2022b). Versatile nanoarchitectonics of Pt with morphology control of oxygen reduction reaction catalysts. *Sci. Technol. Adv. Mater.* 23, 413–423. doi:10.1080/14686996.2022.2088040

Chen, K., Weng, S., Lu, J., Gu, J., Chen, G., Hu, O., et al. (2021c). Facile synthesis of Chitosan derived heteroatoms-doped hierarchical porous carbon for supercapacitors. *Microporous Mesoporous Mater.* 320, 111106. doi:10.1016/j.micromeso.2021.111106

Chen, R., Zhao, T., Zhang, X., Li, L., and Wu, F. (2016). Advanced cathode materials for lithium-ion batteries using nanoarchitectonics. *Nanoscale Horiz.* 1, 423–444. doi:10.1039/c6nh00016a

Chen, Z., Zhuo, H., Hu, Y., Lai, H., Liu, L., Zhong, L., et al. (2020). Wood-derived lightweight and elastic carbon aerogel for pressure sensing and energy storage. *Adv. Funct. Mater.* 30, 1910292. doi:10.1002/adfm.201910292

Eftekhari, K., Parakhonskiy, B. V., Grigoriev, D., and Skirtach, A. G. (2024). Advances in nanoarchitectonics: a review of "static" and "dynamic" particle assembly methods. *Materials* 17, 1051. doi:10.3390/ma17051051

Eguchi, M., Nugraha, A. S., Rowan, A. E., Shapter, J., and Yamauchi, Y. (2021). Adsorchromism: molecular nanoarchitectonics at 2D nanosheets—old chemistry for advanced chromism. *Adv. Sci.* 8, 2100539. doi:10.1002/advs.202100539

Feynman, R. P. (1960). There's plenty of room at the bottom. *Calif. Inst. Technol. J. Eng. Sci.* 4, 23–36.

Fukushima, T., Higashi, M., and Yamauchi, M. (2023). Carbon-neutral energy cycle via highly selective electrochemical reactions using biomass derivable organic liquid energy carriers. *Bull. Chem. Soc. Jpn.* 96, 1209–1215. doi:10.1246/bcsj.20230172

Gao, F., Zhang, J., Ren, M., Ge, Y., Chen, H., Ma, X., et al. (2020). Preparation and characterization of porous carbons by pyrolysis-CO_2 gasification of pine sawdust. *Chem. Lett.* 49, 652–655. doi:10.1246/cl.200087

Gehrke, V., Maron, G. K., Rodrigues, L. D. S., Alano, J. H., Pereira, CMPD, Orlandi, M. O., et al. (2021). Facile preparation of a novel biomass-derived H_3PO_4 and $Mn(NO_3)_2$ activated carbon from citrus Bergamia peels for high-performance supercapacitors. *Mater Today Comm.* 26, 101779. doi:10.1016/j.mtcomm.2020.101779

Gnawali, C. L., Manandhar, S., Shahi, S., Shrestha, R. G., Adhikari, M. P., Rajbhandari, R., et al. (2023a). Nanoporous carbon materials from Terminalia bellirica seed for iodine and methylene blue adsorption and high-performance supercapacitor applications. *Bull. Chem. Soc. Jpn.* 96, 572–581. doi:10.1246/bcsj.20230093

Gnawali, C. L., Shrestha, L. K., Hill, J. P., Ma, R., Ariga, K., Adhikari, M. P., et al. (2023b). Nanoporous activated carbon material from Terminalia chebula seed for supercapacitor application. *C—J Carbon Res* 9, 109. doi:10.3390/c9040109

Guo, D., Shibuya, R., Akiba, C., Saji, S., Kondo, T., and Nakamura, J. (2016). Active sites of nitrogen-doped carbon materials for oxygen reduction reaction clarified using model catalysts. *Science* 351, 361–365. doi:10.1126/science.aad0832

Hassan, M., Mohanty, A. K., and Misra, M. (2024). 3D printing in upcycling plastic and biomass waste to sustainable polymer blends and composites: a review. *Mater. Des.* 237, 112558. doi:10.1016/j.matdes.2023.112558

Hikichi, R., Tokura, Y., Igarashi, Y., Imai, H., and Oaki, Y. (2023). Fluorine-free substrate-independent superhydrophobic coatings by nanoarchitectonics of polydispersed 2D materials. *Bull. Chem. Soc. Jpn.* 96, 766–774. doi:10.1246/bcsj.20230126

Hosaka, T., and Komaba, S. (2022). Development of nonaqueous electrolytes for high-voltage K-ion batteries. *Bull. Chem. Soc. Jpn.* 95, 569–581. doi:10.1246/bcsj.20210412

Hsieh, C.-T., Hsu, S.-H., Maji, S., Chahal, M. K., Song, J., Hill, J. P., et al. (2020). Post-assembly dimension-dependent face-selective etching of fullerene crystals. *Mater Horiz.* 7, 787–795. doi:10.1039/c9mh01866b

Hu, W., Shi, J., Lv, W., Jia, X., and Ariga, K. (2022). Regulation of stem cell fate and function by using bioactive materials with nanoarchitectonics for regenerative medicine. *Sci. Technol. Adv. Mater.* 23, 393–412. doi:10.1080/14686996.2022.2082260

Huang, H., Li, Z., Yin, S., Li, Z., Liu, H., Augustine, A., et al. (2024a). Review and outlook on the utilization of low-concentration coalbed methane for power generation by solid oxide fuel cells. *Energy Fuels.* 38, 1618–1632. doi:10.1021/acs.energyfuels.3c03889

Huang, P., Wu, W., Li, M., Li, Z., Pan, L., Ahamad, T., et al. (2024b). Metal-organic framework-based nanoarchitectonics: a promising material platform for electrochemical detection of organophosphorus pesticides. *Coord. Chem. Rev.* 501, 215534. doi:10.1016/j.ccr.2023.215534

Huang, Y., Peng, L., Liu, Y., Zhao, G., Chen, J. Y., and Yu, G. (2016). Biobased nano porous active carbon fibers for high-performance supercapacitors. *ACS Appl. Mater. and Interfaces* 8, 15205–15215. doi:10.1021/acsami.6b02214

Imahori, H. (2023). Molecular photoinduced charge separation: fundamentals and application. *Bull. Chem. Soc. Jpn.* 96, 339–352. doi:10.1246/bcsj.20230031

Ishii, M., Yamashita, Y., Watanabe, S., Ariga, K., and Takeya, J. (2023). Doping of molecular semiconductors through proton-coupled electron transfer. *Nature* 622, 285–291. doi:10.1038/s41586-023-06504-8

Islam, M. S., Shudo, Y., and Hayami, S. (2022). Energy conversion and storage in fuel cells and super-capacitors from chemical modifications of carbon allotropes: state-of-art and prospect. *Bull. Chem. Soc. Jpn.* 95, 1–25. doi:10.1246/bcsj.20210297

Jia, X., Chen, J., Lv, W., Li, H., and Ariga, K. (2023). Engineering dynamic and interactive biomaterials using material nanoarchitectonics for modulation of cellular behaviors. *Cell Rep. Phys. Sci.* 4, 101251. doi:10.1016/j.xcrp.2023.101251

Jiang, B., Wang, S., Meng, F., Ju, L., Jiang, W., Ji, Q., et al. (2022a). Enhancing the ORR activity of fullerene-derived carbons by implanting Fe in assembled diamine–C_{60} spheres. *Cryst. Eng. Comm.* 24, 5783–5791. doi:10.1039/d2ce00737a

Jiang, Y., He, Z., Cui, X., Liu, Z., Wan, J., Liu, Y., et al. (2022b). Hierarchical porous carbon derived from coal tar pitch by one step carbonization and activation combined with a CaO template for supercapacitors. *New J. Chem.* 46, 6078–6090. doi:10.1039/d2nj00433j

Jiang, Y., Zhang, Z., Zhang, Y., Zhou, X., Wang, L., Yasin, A., et al. (2018). Bioresource derived porous carbon from cottonseed hull for removal of triclosan and electrochemical application. *RSC Adv.* 8, 42405–42414. doi:10.1039/c8ra08332k

Kalinova, R., Mladenova, K., Petrova, S., Doumanov, J., and Dimitrov, I. (2022). Nanoarchitectonics of spherical nucleic acids with biodegradable polymer cores: synthesis and evaluation. *Materials* 15, 8917. doi:10.3390/ma15248917

Kalyana Sundaram, S. D., Hossain, M. M., Rezki, M., Ariga, K., and Tsujimura, S. (2023). Enzyme cascade electrode reactions with nanomaterials and their applicability towards biosensor and biofuel cells. *Biosensors* 13, 1018. doi:10.3390/bios13121018

Kim, J., Kim, J. H., and Ariga, K. (2017). Redox-active polymers for energy storage nanoarchitectonics. *Joule* 1, 739–768. doi:10.1016/j.joule.2017.08.018

Kim, S. K., Lee, J. U., Jeon, M. J., Kim, S.-K., Hwang, S.-H., Hong, M. E., et al. (2023). Bio-conjugated nanoarchitectonics with dual-labeled nanoparticles for a colorimetric and fluorescent dual-mode serological lateral flow immunoassay sensor in detection of SARS-CoV-2 in clinical samples. *RSC Adv.* 13, 27225–27232. doi:10.1039/d3ra04373h

Kimura, K., Miwa, K., Imada, H., Imai-Imada, M., Kawahara, S., Takeya, J., et al. (2019). Selective triplet exciton formation in a single molecule. *Nature* 570, 210–213. doi:10.1038/s41586-019-1284-2

Kinoshita, T. (2022). Highly efficient wideband solar energy conversion employing singlet-triplet transitions. *Bull. Chem. Soc. Jpn.* 95, 341–352. doi:10.1246/bcsj.20210423

Kojima, A., Teshima, K., Shirai, Y., and Miyasaka, T. (2009). Organometal halide perovskites as visible-light sensitizers for photovoltaic cells. *J. Am. Chem. Soc.* 131, 6050–6051. doi:10.1021/ja809598r

Koralkar, N., Mehta, S., Upadhyay, A., Patel, G., and Deshmukh, K. (2024). MOF-based nanoarchitectonics for lithium-ion batteries: a comprehensive review. *J. Inorg. Organomet. Polym.* 34, 903–929. doi:10.1007/s10904-023-02898-0

Laughlin, R. B., and Pines, D. (2000). The theory of everything. *Proc. Natl. Acad. Sci.* 97, 28–31. doi:10.1073/pnas.97.1.28

Liang, H., Zhu, X., Chen, Y., and Cheng, J. (2024). Nanoarchitectonics of yttrium-doped barium cerate-based proton conductor electrolyte for solid oxide fuel cells. *Appl. Phys. A* 130, 168. doi:10.1007/s00339-024-07341-w

Liang, K., Chen, Y., Wang, S., Wang, D., Wang, W., Jia, S., et al. (2023). Peanut shell waste derived porous carbon for high-performance supercapacitors. *J. Energy Storage* 70, 107947. doi:10.1016/j.est.2023.107947

Liu, B., Yang, M., Chen, H., Liu, Y., Yang, D., and Li, H. (2018). Graphene-like porous carbon nanosheets derived from Salvia splendens for high-rate performance supercapacitors. *J. Power Sources* 397, 1–10. doi:10.1016/j.jpowsour.2018.06.100

Liu, B., Ye, Y., Yang, M., Liu, Y., Chen, H., Li, H., et al. (2023b). All-in-one biomass-based flexible supercapacitors with high rate performance and high energy density. *Adv. Funct. Mater.* 34, 2310534. doi:10.1002/adfm.202310534

Liu, H., Chen, W., Zhang, R., and Ren, Y. (2021b). Naturally O-N-S co-doped carbon with multiscale pore architecture derived from lotus leaf stem for high-performance supercapacitors. *Bull. Chem. Soc. Jpn.* 94, 1705–1714. doi:10.1246/bcsj.20210027

Liu, S., Wei, C., Wang, H., Yang, W., Zhang, J., Wang, Z., et al. (2023a). Processable nanoarchitectonics of two-dimensional metallo-supramolecular polymer for electrochromic energy storage devices with high coloration efficiency and stability. *Nano Energy* 110, 108337. doi:10.1016/j.nanoen.2023.108337

Liu, X., Chen, T., Gong, Y., Li, C., Niu, L., Xu, S., et al. (2021a). Light-conversion phosphor nanoarchitectonics for improved light harvesting in sensitized solar cells. *J. Photochem. Photobiol. C Photochem. Rev.* 47, 100404. doi:10.1016/j.jphotochemrev.2021.100404

Liu, Y., Shi, Z., Gao, Y., An, W., Cao, Z., and Liu, J. (2016). Biomass-swelling assisted synthesis of hierarchical porous carbon fibers for supercapacitor electrodes. *ACS Appl. Mater. Interfaces* 8, 28283–28290. doi:10.1021/acsami.5b11558

Lobato-peralta, D. R., Duque-Brito, E., Orugba, H. O., Arias, D. M., Cuentas-Gallegos, A. K., Okolie, J. A., et al. (2023). Sponge-like nanoporous activated carbon from corn husk as a sustainable and highly stable supercapacitor electrode for energy storage. *Diam. Relat. Mater.* 138, 110176. doi:10.1016/j.diamond.2023.110176

Lu, T., Xu, X., Zhang, S., Pan, L., Wang, Y., Alshehri, S. M., et al. (2020). High-performance capacitive deionization by lignocellulose-derived eco-friendly porous carbon materials. *Bull. Chem. Soc. Jpn.* 93, 1014–1019. doi:10.1246/bcsj.20200055

Maji, S., Chaudhary, R., Shrestha, R. G., Shrestha, R. L., Demir, B., Searles, D. J., et al. (2021a). High-performance supercapacitor materials based on hierarchically porous carbons derived from Artocarpus heterophyllus seed. *ACS Appl. Energy Mater* 4, 12257–12266. doi:10.1021/acsaem.1c02051

Maji, S., Shrestha, R. G., Lee, J., Han, S. A., Hill, J. P., Kim, J. H., et al. (2021b). Macaroni fullerene crystals-derived mesoporous carbon tubes as a high rate

performance supercapacitor electrode material. *Bull. Chem. Soc. Jpn.* 94, 1502–1509. doi:10.1246/bcsj.20210059

Meng, R.-Y., Zhao, Y., Xia, H.-Y., Wang, S.-B., Chen, A.-Z., and Kankala, R. K. (2024). 2D architectures-transformed conformational nanoarchitectonics for light-augmented nanocatalytic chemodynamic and photothermal/photodynamic-based trimodal therapies. *ACS Mater. Lett.* 6, 1160–1177. doi:10.1021/acsmaterialslett.3c01615

Miyazawa, K. (2009). Synthesis and properties of fullerene nanowhiskers and fullerene nanotubes. *J. Nanosci. Nanotechnol.* 9, 41–50. doi:10.1166/jnn.2009.j013

Mohammed, A. A., Chen, C., and Zhu, Z. (2019). Low-cost, high-performance supercapacitor based on activated carbon electrode materials derived from baobab fruit shells. *J. Colloid Interface Sci.* 538, 308–319. doi:10.1016/j.jcis.2018.11.103

Mohapatra, D., Dhakal, G., Sayed, M. S., Subramanya, B., Shim, J.-J., and Parida, S. (2019). Sulfur doping: unique strategy to improve the supercapacitive performance of carbon nano-onions. *ACS Appl. Mater Interfaces* 11, 8040–8050. doi:10.1021/acsami.8b21534

Munawar, T., Sardar, S., Mukhtar, F., Nadeem, M. S., Manzoor, S., Ashiq, M. N., et al. (2023). Fabrication of fullerene-supported La_2O_3–C_{60} nanocomposites: dual-functional materials for photocatalysis and supercapacitor electrodes. *Phys. Chem. Chem. Phys.* 25, 7010–7027. doi:10.1039/d2cp05357h

Nayak, A., Unayama, S., Tai, S., Tsuruoka, T., Waser, R., Aono, M., et al. (2018). Nanoarchitectonics for controlling the number of dopant atoms in solid electrolyte nanodots. *Adv. Mater.* 30, 1703261. doi:10.1002/adma.201703261

Oliveira, O. N., Jr, Caseli, L., and Ariga, K. (2022). The past and the future of Langmuir and Langmuir–Blodgett films. *Chem. Rev.* 122, 6459–6513. doi:10.1021/acs.chemrev.1c00754

Prasankumar, T., Salpekar, D., Bhattacharyya, S., Manoharan, K., Yadav, R. M., Campos Mata, M. A., et al. (2022). Biomass derived hierarchical porous carbon for supercapacitor application and dilute stream CO_2 capture. *Carbon* 199, 249–257. doi:10.1016/j.carbon.2022.07.057

Prasanthi, I., Bora, B. R., Raidongia, K., and Datta, K. K. R. (2022). Fluorinated graphene nanosheet supported halloysite nanoarchitectonics: super-wetting coatings for efficient and recyclable oil sorption. *Sep. Purif. Technol.* 301, 122049. doi:10.1016/j.seppur.2022.122049

Reddy, Y. N., De, A., Paul, S., Pujari, A. K., and Bhaumik, J. (2023). *In situ* nanoarchitectonics of a MOF hydrogel: a self-adhesive and pH-responsive smart platform for phototherapeutic delivery. *Biomacromolecules* 24, 1717–1730. doi:10.1021/acs.biomac.2c01489

Roukes, M. (2007). Plenty of room, indeed. *Sci. Am.* 17, 4–11. doi:10.1038/scientificamerican0907-4sp

Sagawa, T., Kobayashi, H., Murata, C., Shichibu, Y., Konishi, K., Hashizume, M., et al. (2022). Catalytic synthesis of oxazolidinones from a chitin-derived sugar alcohol. *Bull. Chem. Soc. Jpn.* 95, 1054–1059. doi:10.1246/bcsj.20220106

Saitow, K. (2024). Bright silicon quantum dot synthesis and LED design: insights into size–ligand–property relationships from slow- and fast-band engineering. *Bull. Chem. Soc. Jpn.* 97, uoad002. doi:10.1093/bulcsj/uoad002

Schlee, P., Hosseinaei, O., Baker, D., Landmér, A., Tomani, P., Mostazo-López, M. J., et al. (2019). From waste to wealth: from kraft lignin to free-standing supercapacitors. *Carbon* 145, 470–480. doi:10.1016/j.carbon.2019.01.035

Selvaraj, A. R., Muthusamy, A., Cho, I., Kim, H. J., Senthil, K., and Prabakar, K. (2021). Ultrahigh surface area biomass derived 3D hierarchical porous carbon nanosheet electrodes for high energy density supercapacitors. *Carbon* 174, 463–474. doi:10.1016/j.carbon.2020.12.052

Shang, Z., An, X., Zhang, H., Shen, M., Baker, F., Liu, Y., et al. (2020). Houttuynia-derived nitrogen-doped hierarchically porous carbon for high-performance supercapacitor. *Carbon* 161, 62–70. doi:10.1016/j.carbon.2020.01.020

Sharma, D., Choudhary, P., Mittal, P., Kumar, S., Gouda, A., and Krishnan, V. (2024). Nanoarchitectonics of non-noble-metal-based heterogeneous catalysts for transfer hydrogenation reactions: detailed insights on different Hydrogen sources. *ACS Catal.* 14, 4211–4248. doi:10.1021/acscatal.3c05844

Shen, X., Song, J., Sevencan, C., Leong, D. T., and Ariga, K. (2022). Bio-interactive nanoarchitectonics with two-dimensional materials and environments. *Sci. Technol. Adv. Mater.* 23, 199–224. doi:10.1080/14686996.2022.2054666

Shimohata, Y., Kanematsu, Y., Rivera Rocabado, D. S., and Ishimoto, T. (2023). Quantum effects of hydrogen nuclei on the nuclear magnetic shielding tensor of ice I_h. *J. Phys. Chem. A* 127, 8025–8031. doi:10.1021/acs.jpca.3c01318

Shinde, P. A., Abbas, Q., Chodankar, N. R., Ariga, K., Abdelkareem, M. A., and Olabi, A. G. (2023a). Strengths, weaknesses, opportunities, and threats (SWOT) analysis of supercapacitors: a review. *J. Energy Chem.* 79, 611–638. doi:10.1016/j.jechem.2022.12.030

Shinde, P. A., Chodankar, N. R., Kim, H.-J., Abdelkareem, M. A., Ghaferi, A. A., Han, Y.-K., et al. (2023b). Ultrastable 1T-2H WS_2 heterostructures by nanoarchitectonics of phosphorus-triggered phase transition for hybrid supercapacitors. *ACS Energy. Lett.* 8, 4474–4487. doi:10.1021/acsenergylett.3c01452

Shrestha, L. K., Hill, J. P., Tsuruoka, T., Miyazawa, K., and Ariga, K. (2013b). Surfactant-assisted assembly of fullerene (C_{60}) nanorods and nanotubes formed at a liquid–liquid interface. *Langmuir* 29, 7195–7202. doi:10.1021/la304549v

Shrestha, L. K., Ji, Q., Mori, T., Miyazawa, K., Yamauchi, Y., Hill, J. P., et al. (2013a). Fullerene nanoarchitectonics: from zero to higher dimensions. *Chem. An Asian J.* 8, 1662–1679. doi:10.1002/asia.201300247

Shrestha, L. K., Shahi, S., Gnawali, C. L., Adhikari, M. P., Rajbhandari, R., Pokharel, B. P., et al. (2022a). Phyllanthus emblica seed-derived hierarchically porous carbon materials for high-performance supercapacitor applications. *Materials* 15, 8335. doi:10.3390/ma15238335

Shrestha, L. K., Shrestha, R. G., Chaudhary, R., Pradhananga, R. R., Tamrakar, B. M., Shrestha, T., et al. (2021a). *Nelumbo nucifera* seed–derived nitrogen-doped hierarchically porous carbons as electrode materials for high-performance supercapacitors. *Nanomaterials* 11, 3175. doi:10.3390/nano11123175

Shrestha, L. K., Shrestha, R. G., Hill, J. P., Tsuruoka, T., Ji, Q., Nishimura, T., et al. (2016). Surfactant-triggered nanoarchitectonics of fullerene C_{60} crystals at a liquid–liquid interface. *Langmuir* 32, 12511–12519. doi:10.1021/acs.langmuir.6b01378

Shrestha, L. K., Shrestha, R. G., Maji, S., Pokharel, B. P., Rajbhandari, R., Shrestha, R. L., et al. (2020b). High surface area nanoporous graphitic carbon materials derived from lapsi seed with enhanced supercapacitance. *Nanomaterials* 10, 728. doi:10.3390/nano10040728

Shrestha, L. K., Shrestha, R. G., Shahi, S., Gnawali, C. L., Adhikari, M. P., Bhadra, B. N., et al. (2023a). Biomass nanoarchitectonics for supercapacitor applications. *J. Oleo Sci.* 72, 11–32. doi:10.5650/jos.ess22377

Shrestha, L. K., Wei, Z., Subramaniam, G., Shrestha, R. G., Singh, R., Sathish, M., et al. (2023b). Nanoporous hollow carbon spheres derived from fullerene assembly as electrode materials for high-performance supercapacitors. *Nanomaterials* 13, 946. doi:10.3390/nano13050946

Shrestha, R. G., Maji, S., Mallick, A. K., Jha, A., Man Shrestha, R., Rajbhandari, R., et al. (2022b). Hierarchically porous carbon from Phoenix dactylifera seed for high-performance supercapacitor applications. *Bull. Chem. Soc. Jpn.* 95, 1060–1067. doi:10.1246/bcsj.20220129

Shrestha, R. G., Maji, S., Shrestha, L. K., and Ariga, K. (2020a). Nanoarchitectonics of nanoporous carbon materials in supercapacitors applications. *Nanomaterials* 10, 639. doi:10.3390/nano10040639

Shrestha, R. L., Chaudhary, R., Shrestha, R. G., Shrestha, T., Maji, S., Ariga, K., et al. (2021b). Washnut seed-derived ultrahigh surface area nanoporous carbons as high rate performance electrode material for supercapacitors. *Bull. Chem. Soc. Jpn.* 94, 565–572. doi:10.1246/bcsj.20200314

Shrestha, R. L., Chaudhary, R., Shrestha, T., Tamrakar, B. M., Shrestha, R. G., Maji, S., et al. (2020c). Nanoarchitectonics of lotus seed derived nanoporous carbon materials for supercapacitor applications. *Materials* 13, 5434. doi:10.3390/ma13235434

Shrestha, R. L., Shrestha, T., Tamrakar, B. M., Shrestha, R. G., Maji, S., Ariga, K., et al. (2020d). Nanoporous carbon materials derived from washnut seed with enhanced supercapacitance. *Materials* 13, 2371. doi:10.3390/ma13102371

Sinha, P., Yadav, A., Tyagi, A., Paik, P., Yokoi, H., Naskar, A. K., et al. (2020). Keratin-derived functional carbon with superior charge storage and transport for high-performance supercapacitors. *Carbon* 168, 419–438. doi:10.1016/j.carbon.2020.07.007

Song, J., Murata, T., Tsai, K.-C., Jia, X., Sciortino, F., Ma, R., et al. (2022). Fullerphene nanosheets: a bottom-up 2D material for single-carbon-atom-level molecular discrimination. *Adv. Mater. Interfaces* 9, 2102241. doi:10.1002/admi.202102241

Song, Y., Qu, W., He, Y., Yang, H., Du, M., Wang, A., et al. (2020). Synthesis and processing optimization of n-doped hierarchical porous carbon derived from corncob for high performance supercapacitors. *J. Energy Storage* 32, 101877. doi:10.1016/j.est.2020.101877

Srinivasan, R., Elaiyappillai, E., Pandian, H. P., Vengudusamy, R., Johnson, P. M., Chen, S.-M., et al. (2019). Sustainable porous activated carbon from Polyalthia longifolia seeds as electrode material for supercapacitor application. *J. Electroanal. Chem.* 849, 113382. doi:10.1016/j.jelechem.2019.113382

Sugimoto, Y., Pou, P., Abe, M., Jelinek, P., Pérez, R., Morita, S., et al. (2007). Chemical identification of individual surface atoms by atomic force microscopy. *Nature* 446, 64–67. doi:10.1038/nature05530

Sun, K., Silveira, O. J., Ma, Y., Hasegawa, Y., Matsumoto, M., Kera, S., et al. (2023). On-surface synthesis of disilabenzene-bridged covalent organic frameworks. *Nat. Chem.* 15, 136–142. doi:10.1038/s41557-022-01071-3

Sutrisno, L., and Ariga, K. (2023). Pore-engineered nanoarchitectonics for cancer therapy. *NPG Asia Mater.* 15, 21. doi:10.1038/s41427-023-00469-w

Tang, Q., Bairi, P., Shrestha, R. G., Hill, J. P., Ariga, K., Zeng, H., et al. (2017). Quasi 2D mesoporous carbon microbelts derived from fullerene crystals as an electrode material for electrochemical supercapacitors. *ACS Appl. Mater Interfaces* 9, 44458–44465. doi:10.1021/acsami.7b13277

Tang, Q., Maji, S., Jiang, B., Sun, J., Zhao, W., Hill, J. P., et al. (2019). Manipulating the structural transformation of fullerene microtubes to fullerene microhorns having microscopic recognition properties. *ACS Nano* 13, 14005–14012. doi:10.1021/acsnano.9b05938

Thmaini, N., Charradi, K., Ahmed, Z., Chtourou, R., and Aranda, P. (2023). Nanoarchitectonics of fibrous clays as fillers of improved proton-conducting membranes for fuel-cell applications. *Appl. Clay Sci.* 242, 107019. doi:10.1016/j.clay.2023.107019

Tian, Y., Ren, Q., Chen, X., Li, L., and Lan, X. (2022). Yeast-based porous carbon with superior electrochemical properties. *ACS Omega* 7, 654–660. doi:10.1021/acsomega.1c05278

Tipplook, M., Tanaka, H., Sudare, T., Hagio, T., Saito, N., and Teshima, K. (2024). Nanoarchitectonics solution plasma polymerization of amino-rich carbon nanosorbents for use in enhanced fluoride removal. *ACS Appl. Mater Interfaces* 16, 7038–7046. doi:10.1021/acsami.3c15172

Tokura, Y., and Kanazawa, N. (2021). Magnetic skyrmion materials. *Chem. Rev.* 121, 2857–2897. doi:10.1021/acs.chemrev.0c00297

Tsuchiya, T., Nakayama, T., and Ariga, K. (2022). Nanoarchitectonics intelligence with atomic switch and neuromorphic network system. *Appl. Phys. Express* 15, 100101. doi:10.35848/1882-0786/ac926b

Tu, J., Qiao, Z., Wang, Y., Li, G., Zhang, X., Li, G., et al. (2023). American ginseng biowaste-derived activated carbon for high-performance supercapacitors. *Int. J. Electrochem. Sci.* 18, 16–24. doi:10.1016/j.ijoes.2023.01.011

Vinayagam, M., Babu, R. S., Sivasamy, A., and Barros, De A. L. F. (2020). Biomass-derived porous activated carbon from Syzgium cumini fruit shells and Chrysopogan zizanioides roots for high-energy density symmetric supercapacitors. *Biomass Bioenergy* 143, 105838. doi:10.1016/j.biombioe.2020.105838

Wang, J., Yang, H., Feng, Y., Gao, X., Zhou, C., Cong, S., et al. (2023). High-performance supercapacitor electrodes from porous rotten wood cellulose-derived carbon via fungi action. *Chem. Lett.* 52, 389–392. doi:10.1246/cl.230092

Wang, J., Zhang, Q., and Deng, M. (2022). Eco-friendly preparation of biomass-derived porous carbon and its electrochemical properties. *ACS Omega* 7, 22689–22697. doi:10.1021/acsomega.2c02140

Wang, L., Wu, J., Zhang, C., Cao, X., Xu, X., Bai, J., et al. (2024). Rational nanoarchitectonics of polypyrrole/graphene/polyimide composite fibrous membranes with enhanced electrochemical performance as self-supporting flexible electrodes for supercapacitors. *J. Energy Storage* 81, 110425. doi:10.1016/j.est.2024.110425

Xu, T., Chen, N., He, Z., Yu, P., Shen, W., Akasaka, T., et al. (2021). Morphology engineering of fullerene[C_{70}] microcrystals: from perfect cubes, defective hoppers to novel cruciform-pillars. *Chem. A Eur. J.* 27, 10387–10393. doi:10.1002/chem.202100958

Yoshino, A. (2022). The lithium-ion battery: two breakthroughs in development and two reasons for the Nobel prize. *Bull. Chem. Soc. Jpn.* 95, 195–197. doi:10.1246/bcsj.20210338

Zhang, G., Bai, Q., Wang, X., Li, C., Uyama, H., and Shen, Y. (2023). Preparation and mechanism investigation of walnut shell-based hierarchical porous carbon for supercapacitors. *Bull. Chem. Soc. Jpn.* 96, 190–197. doi:10.1246/bcsj.20220314

Zhang, H., Xiao, W., Zhou, W., Chen, S., and Zhang, Y. (2019). Hierarchical porous carbon derived from sichuan pepper for high-performance symmetric supercapacitor with decent rate capability and cycling stability. *Nanomaterials* 9, 553. doi:10.3390/nano9040553

Zhang, M., and Peng, L. (2024). Research progress of biomass-derived carbon for the supercapacitors. *Mater Res. Express* 11, 012004. doi:10.1088/2053-1591/ad1013

Zhang, S., Li, Y., Du, Y., Ma, X., Lin, J., and Chen, S. (2022). Apple-pomace-based porous biochar as electrode materials for supercapacitors. *Diam. Relat. Mater.* 130, 109507. doi:10.1016/j.diamond.2022.109507

Zhang, S., Tamura, A., and Yui, N. (2024). Supramolecular nanoarchitectonics of propionylated polyrotaxanes with bulky nitrobenzyl stoppers for light-triggered drug release. *RSC Adv.* 14, 3798–3806. doi:10.1039/d4ra00213j

Zhu, Y., Chen, M., Zhang, Y., Zhao, W., and Wang, C. (2018). A biomass-derived nitrogen-doped porous carbon for high-energy supercapacitor. *Carbon* 140, 404–412. doi:10.1016/j.carbon.2018.09.009